10

Global View of Remote Sensing of Rangelands: Evolution, Applications, Future Pathways

Matthew C. Reeves
U.S.D.A Forest Service

Robert A. Washington-Allen
University of Tennessee

Jay Angerer
Texas A&M University

E. Raymond Hunt, Jr.
USDA-ARS Beltsville Agricultural Research Center

Ranjani Wasantha Kulawardhana
Texas A&M University

Lalit Kumar
University of New England

Tatiana Loboda
University of Maryland

Thomas Loveland
U.S. Geological Survey EROS Center

Graciela Metternicht
University of New South Wales

R. Douglas Ramsey
Utah State University

Acronyms and Definitions

AATSR	Advanced Along-Track Scanning Radiometer
AI	Aridity Index
ANPP	Aboveground net primary productivity
ASSOD	Assessment of the Status of Human-induced Soil Degradation in South and Southeast Asia
ATSR	Along-Track Scanning Radiometer
AUM	Animal unit month
AVHRR	Advanced Very High Resolution Radiometer
BRDF	Bidirectional reflectance distribution function
BT	Brightness temperature
CBI	Composite burn index
CSIRO	Commonwealth Scientific and Industrial Research Organization

DISCover	International Geosphere-Biosphere Programme Data and Information System, Global Land Cover Classification
DLDD	Desertification, land degradation, and drought
dNBR	Differenced normalized burn ratio
EDR	Environmental Data Record
Eionet	European Environment Information and Observation Network
EM	Electromagnetic
ENVISAT	Environmental Satellite
EOS	Earth Observing System
ERS-2	European Remote Sensing (satellite)
ERTS	Earth Resources Technology Satellite
ESA	European Space Agency
ETM+	Enhanced Thematic Mapper Plus
EVI	Enhanced vegetation index
FAO	Food and Agricultural Organization of the United Nations
fPAR	Fraction of Photosynthetically Active Radiation
FRE	Fire radiative energy (in Joules)
FROM-GLC	Fine Resolution Observation and Monitoring of Global Land Cover
FRP	Fire radiative power (in Watts)
GAC	Global Area Coverage
GDAS	Global Data Assimilation System
GEF	Global Environmental Facility
GEO-5	Fifth Global Environment Outlook
GEO BON	Group on Earth Observations Biodiversity Observation Network
GIMMS	Global Inventory Modeling and Mapping Studies
GIS	Geographic information system
GLADA	Global Assessment of Land Degradation and Improvement
GLADIS	Global Land Degradation Information System
GLASOD	Global assessment of human-induced soil degradation
GLC2000	Global Land Cover 2000
GPP	Gross primary production
GVMI	Global Vegetation Moisture Index
HRVIR	Haute Résolution dans le Visible et l'Infra-Rouge (French)
IDRISI	a geographic information system and remote sensing software produced by Clark University
IGBP	International Geosphere–Biosphere Programme
IRS	Indian Remote Sensing
J	Joules
JPSS	Joint Polar Satellite System
LADA	Land Degradation Assessment in Drylands
LAI	Leaf area index
LCCS	Land cover classification system
LEWS	Livestock Early Warning System
LNS	Local net primary productivity scaling
LUS	Land use system
LWCI	Leaf Water Content Index
LWIR	Long Wave Infrared
MEA	Millennium Ecosystem Assessment
MERIS	Medium Resolution Imaging Spectrometer
MODIS	Moderate Resolution Imaging Spectroradiometer
MSI	Moisture Stress Index
MSS	Multispectral Scanner
MTBS	Monitoring Trends in Burn Severity
MWIR	Mid-wave Infrared
NASA	National Aeronautics and Space Administration
NDBR	Normalized difference burn ratio
NDII	Normalized Difference Infrared Index
NDVI	Normalized Difference Vegetation Index
NDWI	Normalized Difference Water Index
NIR	Near infrared (0.7–1.0 μm)
NLCD	National Land Cover Database
NOAA	National Oceanic and Atmospheric Administration
NPoP	National Polar-orbiting Partnership
NPP	Net primary productivity
NWCG	National Wildfire Coordinating Group
OLI	Optical Land Imager
P	Precipitation
PET	Potential Evapotranspiration
PHYGROW	Phytomass Growth Simulation Model
PSNnet	Moderate Resolution Imaging Spectroradiometer net photosynthesis product
RdNBR	Relativized differenced normalized burn ratio
Rio+20	United Nations Conference on Sustainable Development
RUE	Rain use efficiency
SAVI	Soil Adjusted Vegetation Index
SDGs	Sustainable development goals
SSI	Soil Stability Index
SST	Sea Surface Temperature
SOVEUR	Mapping of Soil and Terrain Vulnerability in Central and Eastern Europe
SPOT	Satellite Pour l'Observation de la Terre (French)
SWIR	Shortwave infrared (1.1–2.4 μm)
$SWIR_{2.2}$	Shortwave infrared (2.08–2.35 μm)
Tg	teragrams
TIROS-N	Television Infrared Observation Satellite-Next Generation
TIRS	Thermal Infrared Sensor
TM	Thematic Mapper (Landsat)
TNDVI	Transformed Normalized Difference Vegetation Index
TVI	Transformed Vegetation Index
UMD	University of Maryland
UNCCD	United Nations Convention to Combat Desertification
UNEP	United Nations Environment Program
USFWS	United States Fish and Wildlife Service
USGS	United States Geological Survey
VASClimO	Variability Analyses of Surface Climate Observations
VGT	VEGETATION sensor onboard SPOT satellite
VI	Vegetation Index

VIIRS	Visible Infrared Imaging Radiometer Suite
W	Watts
WHR	Wildlife Habitat Relationship

10.1 Introduction

The term "rangeland" is rather nebulous, and there is no single definition of rangeland that is universally accepted by land managers, scientists, or international bodies (Lund, 2007; Reeves and Mitchell, 2011). Dozens and possibly hundreds (Lund, 2007) of definitions and ideologies exist because various stakeholders often have unique objectives requiring different information. For the purpose of describing the role of remote sensing in a global context, it is, however, necessary to provide definitions to orient the reader. The Food and Agricultural Organization (FAO) of the United Nations convened a conference in 2002 and again in 2013 to begin addressing the issue of harmonizing definitions of forest-related activities. Based on this concept, here rangelands are considered lands usually dominated by nonforest vegetation. The Society for Range Management defines rangelands as (SRM, 1998)

> Land on which the indigenous vegetation (climax or natural potential) is predominantly grasses, grass-like plants, forbs, or shrubs and is managed as a natural ecosystem. If plants are introduced, they are managed similarly. Rangelands include natural grasslands, savannas, shrublands, many deserts, tundra, alpine communities, marshes, and wet meadows.

Rangelands occupy a wide diversity of habitats and are found on every continent except Antarctica. Excluding Antarctica and barren lands, rangelands occupy 52% of the Earth's surface based on the land cover analysis presented in Figure 10.1. Figure 10.1 is based on the 2005 Moderate Resolution Imaging Spectroradiometer (MODIS) Collection 4.5, 1 km^2 land cover (the University of Maryland [UMD] classification), and suggested rangeland classes for this dataset are closed shrubland, open shrubland, woody savanna, savanna, and grassland. Using these classes, Russia, Australia, and Canada are the top three countries with the most rangelands (Table 10.1) representing 18%, 10%, and 8% of the global extent, respectively. Th large areal extent of rangelands, high cost of field data collection, and quest for societal well-being have, for decades, provided rich opportunity for remote sensing to aid in answering pressing questions.

10.2 History and Evolution of Global Remote Sensing

The application of digital remote sensing to rangelands is as long as the history of digital remote sensing itself. Before the launch of the Earth Resources Technology Satellite (ERTS)—later renamed Landsat—scientists were evaluating the use of multispectral aerial imagery to map soils and range vegetation (Yost and Wenderoth, 1969). During the late 1960s, the promise of ERTS, designed to drastically improve our ability to update maps and study Earth resources, particularly in developing countries, was eagerly anticipated by a number of government agencies (Carter, 1969). With the ERTS launch on July 23, 1972, a flurry of research activity aimed at the application of this new data source to map Earth resources began. Practitioners who pioneered the use of satellite-based digital remote sensing found the new data source a significant value for rangeland assessments (e.g., Rouse et al., 1973, 1974; Bauer, 1976). This early work established many of the basic techniques still in use today to assess and monitor global rangelands. The following subsections discuss the evolution of remote-sensing data, methods, and approaches in various decades.

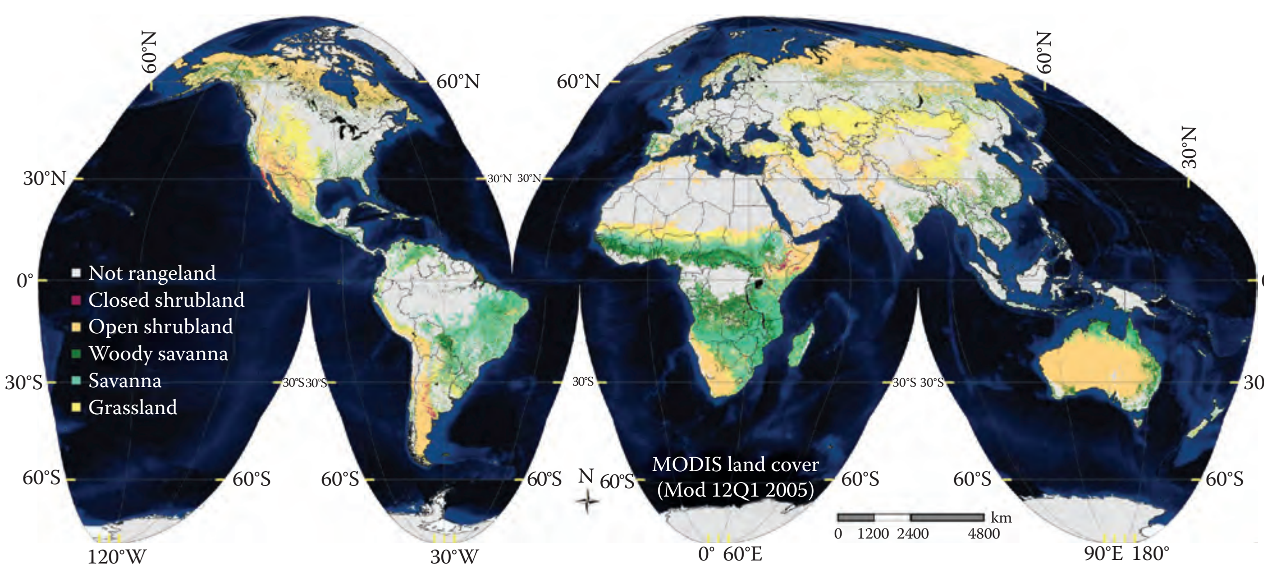

Figure 10.1 Global distribution of land cover types (MODIS MOD12Q1, 2005; University of Maryland Classification), considered rangelands for this chapter.

TABLE 10.1 Global Area of Rangeland Vegetation Types Estimated Using MODIS Land Cover Data (Mod12Q1) for the Top 12 Countries with the Most Rangeland.

Country	Area (km^2)	CSL	Grassland	OSL	Savanna	Woody Savanna	Rangeland Area	Rangeland Proportion (%)
Russia	16,851,940	5,461	795,938	8,174,738	170,456	1,223,381	10,369,974	62
Australia	7,706,142	13,543	182,983	4,690,912	505,136	620,265	6,012,839	78
Canada	9,904,700	1,187	271,855	3,901,991	54,738	509,117	4,738,888	48
United States	9,450,720	78,929	1,777,542	2,077,055	95,380	673,199	4,702,105	50
China	9,338,902	42,548	1,745,760	1,002,771	73,717	399,032	3,263,828	35
Brazil	8,507,128	15,879	278,859	136,105	1,852,468	541,479	2,824,790	33
Kazakhstan	2,715,976	512	1,793,967	171,930	1,859	14,538	1,982,806	73
Argentina	2,781,013	88,877	363,509	1,094,845	121,035	94,377	1,762,643	63
Mexico	1,962,939	64,011	217,212	556,928	85,889	194,310	1,118,350	57
Sudan	2,490,409	8,210	278,848	205,781	404,276	163,169	1,060,284	43

CSL is closed shrubland, OSL is open shrubland, and rangeland proportion is the rangeland area column divided by the area column multiplied by 100.

10.2.1 Beginning of Landsat MSS Era, 1970s

In this first decade of satellite-based digital remote sensing, rangeland scientists quickly assessed the capabilities of this new tool across the globe (Rouse et al., 1973; Graetz et al., 1976). Work by Rouse et al. (1973), in what would later become the Normalized Difference Vegetation Index (NDVI) (Rouse et al., 1974), applied multitemporal ERTS (Landsat 1) at 79 m^2 spatial resolution data to the grasslands of the central Great Plains of the United States and documented that the normalized ratio of the multispectral scanner (MSS) near-infrared (NIR) (band 7) and red band (band 5) was sensitive to vegetation dry biomass, percent green, and moisture content (Figure 10.2). They also determined that within uniform grasslands, field-based estimates of moisture content and percent green cover accounted for 99% of the variation in their "Transformed Vegetation Index" (TVI). The TVI was later renamed to the Transformed Normalized Difference Vegetation Index (TNDVI) (Deering et al., 1975) and is calculated as the square root of the NDVI plus an arbitrary constant (0.5 in their case). This transformation of the NDVI was done to avoid negative values.

The NDVI is, to date, one of the most widely used vegetation index on a global basis. Figure 10.2 shows the graphic published by Rouse et al. (1973) identifying the tight relationship between field-derived green biomass and the TVI. The significance of Figure 10.2 is the demonstration of potential to track vegetation growth across time, thus documenting the ability for remote-sensing instruments to monitor vegetation dynamics and the importance of systematic and uninterrupted collection of remotely sensed imagery.

Another significant development during this first decade of satellite-based remote sensing was the "tasseled cap transformation" (Kauth and Thomas, 1976). The tasseled cap (or "Kauth–Thomas transformation" to some) employed principal component analysis to understand the covariate nature of the four MSS spectral bands and extract from those data the primary ground features, or components, influencing the spectral signature. The tasseled cap and its eventual successor—the brightness, greenness, wetness transform (Crist and Cicone, 1984) applied to the Landsat Thematic Mapper (TM) sensor—has been a widely used tool for many land resource applications (Hacker, 1980; Graetz et al., 1986; Todd et al., 1998).

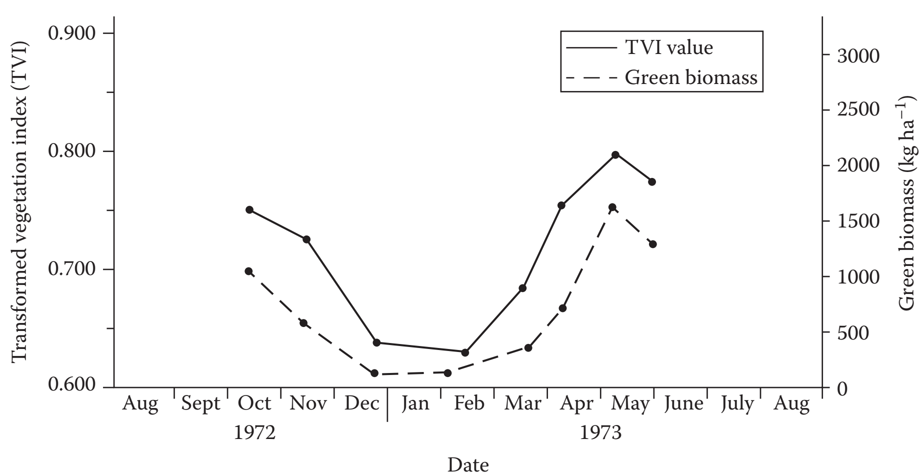

FIGURE 10.2 ERTS-1 TVI values versus green biomass. (Original from Rouse, J.W. et al., Monitoring vegetation systems in the Great Plains with ERTS, in *Proceedings of the Third ERTS Symposium*, Washington, DC, 1973, pp. 309–317.)

The NDVI and the tasseled cap provided the ability to convert reflectance values collected across multiple spectral bands into biophysically focused data layers, thus giving range managers and ecologists a tool by which to directly assess and monitor vegetation growth.

10.2.2 Multiple Sensor Era, 1980s

With the development of the NDVI and the launch of the Television Infrared Observation Satellite-Next Generation (TIROS-N) satellite carrying the Advanced Very High Resolution Radiometer (AVHRR) in October of 1978, remote-sensing practitioners now had the means to monitor temporal vegetation dynamics across very large areas (Tucker, 1979). The 1 km^2 resolution of the AVHRR was ideal for continental-scale monitoring, which was not possible with Landsat images given the computing power and data storage capacities of that era. Further, a 1-day global repeat cycle provided the ability to track phenological changes in vegetation growth within and between years—a feature also not possible with the 18- and 16-day repeat cycles of the Landsat platforms. Gray and McCrary (1981) showed the utility of the AVHRR for vegetation mapping and noted that vegetation indices derived from this sensor could be related to plant growth stress due to water deficits. This relationship, coupled with the high temporal repeat interval of the TIROS-N, led to the use of the NDVI to monitor the impact of drought on grasslands across the Sahel region of Africa (Tucker et al., 1983) and by direct inference predict the impact of drought to local human populations (Prince and Tucker, 1986).

The application of the NDVI to semiarid landscapes was somewhat problematic due to generally low vegetation canopy cover in these environments and the fact that background soil brightness tended to influence the resulting NDVI values (Elvidge and Lyon, 1985). The soil-adjusted vegetation index (SAVI) (Huete, 1988) was developed as a simple modification to the NDVI to account for the influence of soil on the reflectance properties of green vegetation. The SAVI has been used widely within semiarid environments where vegetation cover is low. The 1980s also saw great strides in satellite-based terrestrial remote sensing with the launch of Landsat 4 in July of 1982 and Landsat 5 in March of 1985, as well as the launch of the French Satellite Pour l'Observation de la Terre (SPOT) in 1986. Each platform carried sensors with slightly different capabilities, but each focused their spectral resolution on the red and NIR portions of the electromagnetic spectrum, save one. The Landsat TM was a significant improvement over its predecessor, the MSS. Not only were the spatial and radiometric resolutions improved, but also the TM supported two additional spectral bands calibrated to the shortwave infrared portion of the electromagnetic (EM) spectrum. This significant addition provided the ability to monitor leaf moisture (Tucker, 1980, Hunt and Rock, 1989) as well as identify and map recent wildfires (Chuvieco and Congalton, 1988, Key and Benson, 1999a,b).

While the work with AVHRR in Africa expanded and new sensors were becoming readily available, researchers in Australia were evaluating the applicability of Landsat images to monitoring and assessment of rangelands. Work by Dean Graetz, now retired from the Commonwealth Scientific and Industrial Organisation (CSIRO) of Australia, was instrumental in fostering use of satellite remote sensing to monitor rangelands (Graetz et al., 1983, 1986, 1988; Pech et al., 1986; Graetz, 1987). This work, coupled with other CSIRO scientists such as Geoff Pickup (Pickup and Nelson, 1984; Pickup and Foran, 1987; Pickup and Chewings, 1988), firmly established Australia as a leader in the use of remote sensing for rangeland monitoring and assessment.

Researchers in Australia had similar problems applying digital imagery to semiarid rangelands as did the United States and Africa teams. The difficulty in applying imagery collected by the Landsat sensors to rangeland assessment is documented by Tueller et al. (1978) and McGraw and Tueller (1983), who found that the spectral differences among semiarid range plant communities were so small that they approached the noise level of the imagery. Even with these limitations, Robinove et al. (1981) and Frank (1984) developed methodologies for using albedo to measure soil erosion on rangelands. Pickup and Nelson (1984) developed the soil stability index (SSI) by using the ratio of the MSS green band divided by the NIR, plotted against the ratio of the red divided by the NIR. This comparison between the two ratios provided a quantitative measure of soil stability. Further, a temporal sequence of SSI images could be used as a monitoring tool to identify changes in landscape state (Pickup and Chewings, 1988). As research progressed in the use of imagery on rangelands through the 1980s, the US civilian remote-sensing program began a transition to private sector management of the Landsat program. Issues of data cost and data licensing arose placing financial and legal limitations on research and data sharing. Still, research and application continued into the 1990s with an increased demand by federal land managers for landscape-level information.

10.2.3 Advanced Multisensor Era, 1990s

In 1989 and throughout the 1990s, the US Fish and Wildlife Service (USFWS) and the US Geological Survey (USGS) embarked on a number of large-scale land cover mapping efforts across the United States. The Gap Analysis Program initiated by the USFWS and later absorbed into the USGS was designed as a spatial database to identify landscapes of high biological diversity and evaluate their management status (Scott et al., 1993). The Gap Analysis was built around the linkage between wildlife habitat relationship (WHR) models and a detailed land cover map. This linkage allowed the WHR database to be spatially visualized by relating habitat parameters to land cover. The significance of this effort to remote sensing is that at the time, no one had attempted to map vegetation across landscapes requiring multiple frames of radiometrically normalized satellite imagery. The first digitally produced land cover map derived from a statistical classification of a 14-image mosaic of radiometrically normalized Landsat TM imagery was completed for the state of Utah in 1995 by Utah State University (Homer et al., 1997). Programs like the Gap Analysis, coupled with the advent of the publicly available Internet in 1991, provided the impetus for a new brand of remote sensing centering on large data and improved data access and product delivery. During the late 1980s, the National Aeronautics and Space Administration (NASA) was envisioning the need to provide rapid data access to users. At the time, image acquisition and delivery to the end user required a minimum of a few weeks. There was a need for time critical imagery by users and to meet that demand; NASA set a goal of data delivery to within 24 h of acquisition. Even with the advent of data transfer through the Internet, a 24-h lag between acquisition and delivery is a relatively new phenomenon of the mid-2000s.

10.2.4 New Millennium Era, 2000s

In this era, noteworthy changes to the remote-sensing community, including dramatic improvements in data availability, spatial and spectral resolution, and temporal frequency (Figure 10.3), were made. Commonly used high-spatial-resolution sensors launched during this time including IKONOS, QuickBird, GeoEye-1, and WorldView-2 exhibit spatial resolutions in the multispectral domain of 4, 2.4, 1.65, and 2 m^2, respectively.

These sensors have enabled improvements in species discrimination (e.g., Everitt et al., 2008; Mansour et al., 2012) and stand-level attributes such as canopy cover (e.g., Sant et al., 2014). Use of QuickBird for identifying giant reed (*Arundo donax*) improved both user's and producer's accuracy by an average of 12% over use of SPOT 5 alone (Everitt et al., 2008). Similarly, Sant et al. (2014) used IKONOS imagery to quantify percent vegetation cover and explained 5% more variation than using Landsat (r^2 of 0.79 versus 0.84) alone. Hyperspectral data emanating from this era also enable greater discrimination of many biophysical features than multispectral sensors alone especially in the realm of invasive species mapping. Parker and Hunt (2004) distinguished leafy spurge with the Airborne Visible/Infrared Imaging Spectrometer (AVIRIS) data with overall accuracy of 95%, while Oldeland et al. (2010) detected bush encroachment by *Acacia* spp. ($r^2 = 0.53$). These improved capabilities emanate not only from improved sensor characteristics in the 2000s, but also greatly improved data availability.

In 1999, the launch of Landsat 7, coupled with new sensors from a host of other countries as well as commercial, high-spatial-resolution sensors, ushered a new era of global assessment and monitoring of natural and human landscapes. With the end of private sector management of the Landsat program in 1999, imagery was again placed in the public domain, and costs for Landsat

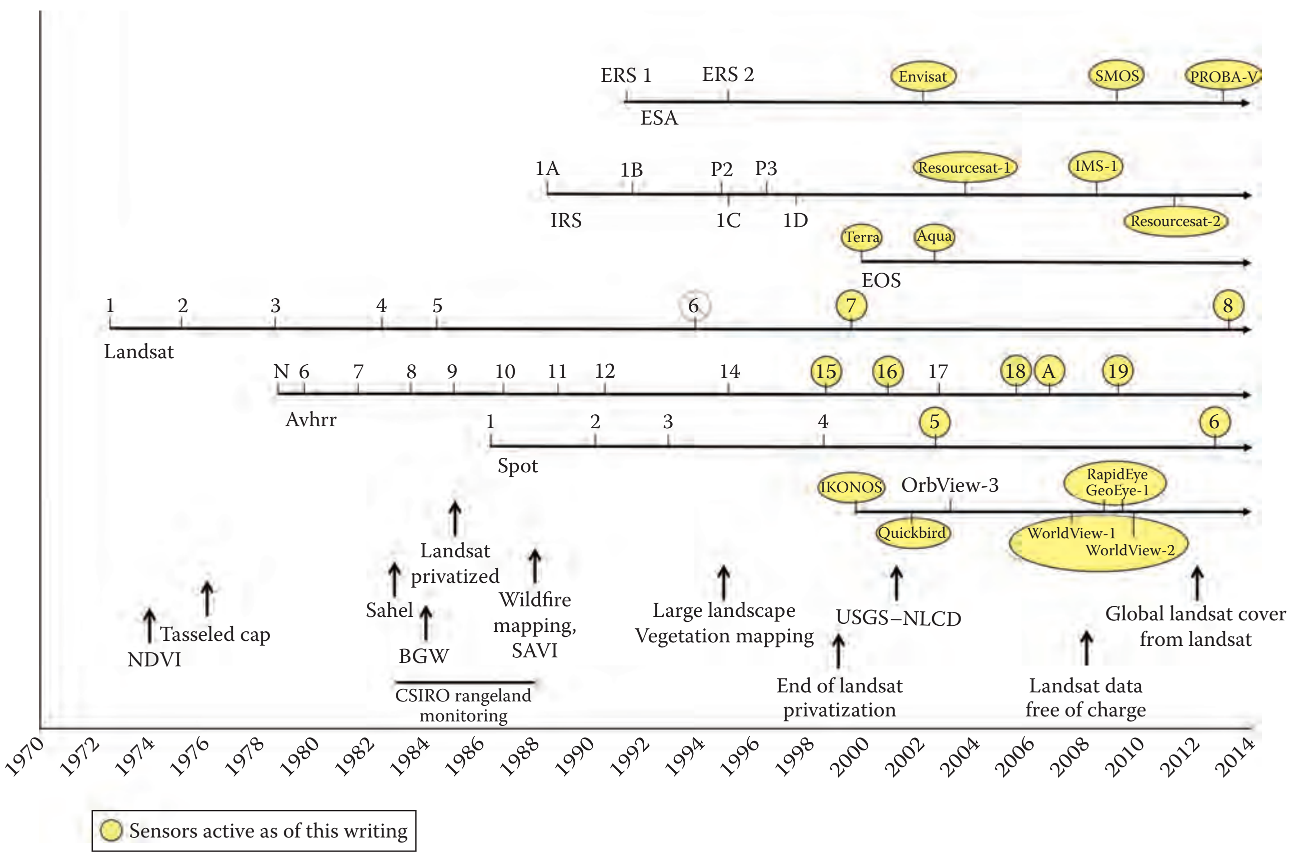

Figure 10.3 History of digital remote sensing sensors used in research and monitoring of rangelands since the advent of the technology in the early 1970's. Specific research milestones and policy changes are also noted.

imagery were reduced to $600 per scene (previously set at $4400 per scene) for Landsat 7 Enhanced Thematic Mapper Plus (ETM+) imagery and $450 per scene for Landsat 5 TM. This reduction in cost, coupled with the free exchange of data between collaborators, boosted research and application of satellite remote sensing. Further, the replacement of the AVHRR as the primary global sensor with the much-advanced MODIS with 36 spectral bands spanning the 405–14,384 nm range provided the ability for scientists to model, map, and monitor not only land cover but also net primary productivity (NPP) among other metrics. The now 15-year history of the MODIS sensor aboard two platforms (Terra and Aqua) has provided an unprecedented source of global land cover dynamics data freely available to land managers and scientists. In 2008, the USGS made all Landsat data accessed through the Internet free of charge. With this policy change, scene requests at the USGS Earth Resources Observation and Science Center jumped from 53 images per day to about 5800 images per day. This increase in data demand and delivery has arguably resulted in research in the 2000s centered on the copious use of imagery across multiple temporal and landscape scales. Commercial satellites such as the IKONOS, launched in 1999, QuickBird in 2001, and the WorldView and GeoEye satellites launched between 2007 and 2009 has provided on-demand access to high spatial resolution (submeter to a few meters) that allows data integration between a wide array of platforms and spatial scales (Sant et al., 2014).

10.3 State of the Art

Millions of people depend on rangelands for their livelihood. This dependence raises numerous concerns about the health, maintenance, and management of rangelands from local to global perspectives. Discerning and describing how rangelands are changing at multiple spatial and temporal scales requires the integration of sensors that possess specific characteristics. The current suite of government-sponsored and commercial sensors suitable for regional to global analysis span the spatial range of submeter to 1 km^2, a temporal range of daily to bimonthly (temporal resolution is inversely proportional to spatial resolution), and all have the capacity to image landscapes in the visible and NIR (Figure 10.4). The most commonly used sensors for global applications, however, have spatial resolutions of between 250 and 1000 m^2 (e.g., MODIS, AVHRR, and Visible Infrared Imaging Radiometer Suite [VIIRS]) and exhibit high temporal frequency, numerous spectral bands, but relatively low spatial resolution. Sensors best suited for regional to local applications (e.g., Landsat, SPOT, WorldView, and GeoEye) have higher spatial resolutions (submeter to 30 m^2) and lower temporal repeat cycles.

The present role of remote sensing for characterizing five globally significant phenomena are discussed hereafter, including land degradation, fire, food security, land cover, and vegetation response to global change (Table 10.2). These factors

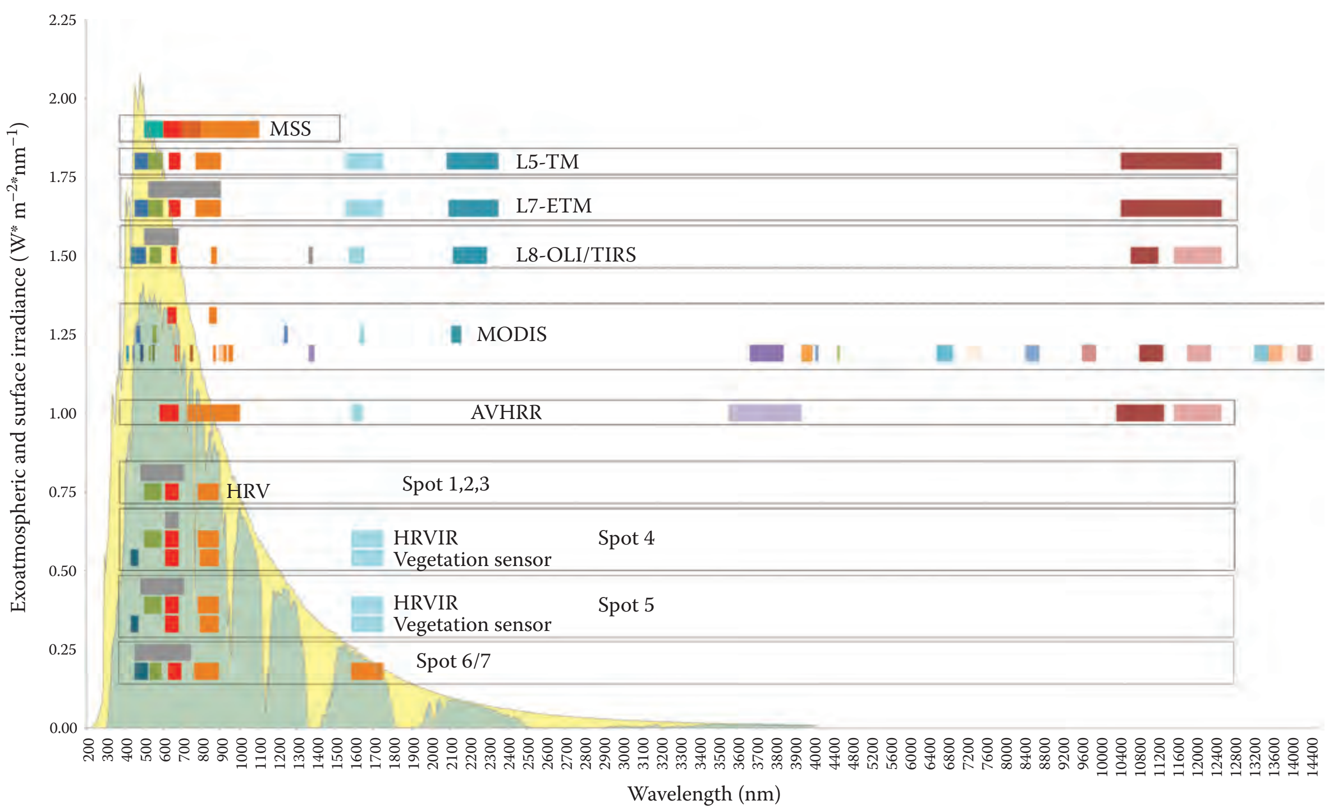

Figure 10.4 Exoatmosphreic and surface irradiance for wavelengths across the electromagnetic spectrum and the bandpasses of sensors (colored squares within each sensor box) commonly used for rangeland studies and monitoring.

TABLE 10.2 Four Most Common Sensors for Regional and Global Applications, Their Characteristics, and Example Applications

Satellite (Sensors)	Characteristics (a Is Spatial Resolution, b Is Launch Date, c Is Swath Width, and d Is Revisit Time)	Rangeland Application Examples	References
Landsat (5, 7, 8) (Thematic Mapper, Enhanced Thematic Mapper Plus [ETM+], Optical Land Imager [OLI])	(a) 15 (panchromatic), 30 (multispectral), 100 (thermal), (b) 1999 (ETM+) and 2013 (OLI), (c) 185 km × 170 km, and (d) 16 days	Fire (often dNBR, NBR, LWCI)	
		Burn severity (dNBR, RdNBR, tasseled cap brightness)	Key and Benson (2006), Miller and Thode (2007), and Loboda et al. (2013)
		Burned area mapping (Eidenshenk et al., 2007)	Eidenshink et al. (2007)
		Fuel moisture (variety of indices such as NDVI, NDII, and LWCI)	Chuvieco et al. (2002)
		Vegetation attributes	
		Land cover (varied methods)	Gong et al. (2013), Fry et al. (2011), and Rollins (2009)
		Leaf area index (LAI)/Fraction of Photosynthetically Active Radiation (fPAR) absorbed by vegetation (radiative transfer and vegetation indices)	Shen et al. (2014)
		Net primary production (NPP) (multisensor fusion and process modeling)	Li et al. (2012)
		Degradation (change detection and residual trend analysis)	Jabbar and Zhou (2013)
SPOT (VEGETATION)	(a) 1000, (b) 1998, (c) 2250 km, and (d) 1–2 days	Fire	
		Burned area mapping dNBR (NDVI, NDWI)	Silva et al. (2005) and Tansey et al. (2004)
		Fuel moisture (primarily NDVI, NDWI)	Verbesselt et al. (2007)
		Vegetation attributes	
		Land cover (GLC2000)	Bartholomé and Belward (2005)
		NPP/abundance (NDVI, process modeling)	Telesca and Lasaponara (2006), Geerken et al. (2005), and Jarlan et al. (2008)
		Degradation (trend analysis)	Fang and Ping (2010)
Aqua and Terra (Moderate Resolution Imaging Spectroradiometer)	(a) 250 (red, NIR), 500 (multispectral), 1000 (multispectral); (b) 2000 (Terra), 2002 (Aqua); (c) 2230 km; and (d) 1–2 days	Fire (often dNBR, NBR, LWCI)	
		Active fi e detection (thermal anomalies and fi e radiative potential)	Giglio et al. (2003, 2009)
		Burned area evaluation (SWIR VI and change detection)	Roy et al. (2008)
		Burn severity (time-integrated dNBR)	Veraverbeke et al. (2011)
		Fuel moisture (empirical relations and radiative transfer modeling; many vegetation indices [GVMI,NDWI, MSI, etc.])	Yebra et al. (2008) and Sow et al. (2013)
		Vegetation attributes	
		Land cover (varied methods)	Friedl et al. (2010)
		LAI/fPAR absorbed by vegetation (radiative transfer modeling)	Myneni et al. (2002) and Wenze et al. (2006)
		NPP (process modeling)	Running et al. (2004), Reeves et al. (2006), Zhao et al. (2011)
		Degradation (rain use effici cy, local NPP scaling, trend and condition analysis)	Bai et al. (2008), Prince et al. (2009), and Reeves and Bagget (2014)
		Livestock Early Warning System (time series analysis of NDVI, and biomass)	Angerer (2012) and Yu et al. (2011)

(*Continued*)

TABLE 10.2 (*Continued*) Four Most Common Sensors for Regional and Global Applications, Their Characteristics, and Example Applications

Satellite (Sensors)	Characteristics (a Is Spatial Resolution, b Is Launch Date, c Is Swath Width, and d Is Revisit Time)	Rangeland Application Examples	References
National Oceanic and Atmospheric Administration (Advanced Very High Resolution Radiometer)	(a) 1000 m, (b) NOAA-15 (1998), NOAA-16 (2000), NOAA-18 (2005), NOAA-19 (2009) satellite series (1980 to present). The approximate scene size is 2400 km × 6400 km	Fire	
		Active fi e detection (thermal anomalies and NDVI)	Pu et al. (2004), Flasse and Ceccato (1996), and Dwyer et al. (2000)
		Burned area evaluation (multitemporal multithreshold approach)	Barbosa et al. (1999)
		Fuel moisture (NDVI)	Paltridge and Barber (1988) and Eidenshink et al. (2007)
		Vegetation attributes	
		Land cover (unsupervised and supervised time series analysis)	Loveland et al. (2000) and Hansen et al. (2000)
		LAI/fPAR absorbed by vegetation (radiative transfer modeling, feedforward neural network)	Myneni et al., (2002), Ganguly (2008), and Zhu and Southworth (2013)
		NPP (time-integrated NDVI)	An et al. (2013)
		Degradation (NDVI and rainfall use efficiency)	Wessels et al. (2004) and Bai et al. (2008)

Many sensors that may have use for evaluating rangeland are not included. Svoray et al. (2013) provide a larger number of example applications in rangeland environments, but this table focuses largely on globally applicable sensors and global applications.

are not mutually exclusive and often exhibit significant interaction. Using remote sensing at global scales provides insight to what may be anticipated in the future and indicates regions where ecological thresholds have been crossed, beyond which decreased goods and services from rangelands can be expected.

10.3.1 Rangeland Degradation

Land and soil degradation are accelerating, and drought is escalating worldwide. At the UN Conference on Sustainable Development (Rio+20), world leaders acknowledged that desertification, land degradation, and drought (DLDD) are challenges of a global dimension affecting the sustainable development of all countries, especially developing countries. Drylands are often identified and classified according to the aridity index (AI), which is defined as P/PET where P is the annual precipitation and PET is the potential evapotranspiration. Drylands yield AI values ≤0.65. Despite decades of research, standards to measure progression of land degradation (e.g., global mapping and monitoring systems) remain elusive, but remote sensing plays a significant role.

10.3.1.1 Soil and Land Degradation and Desertification: What Is the Difference?

Land degradation and desertification have been sometimes used synonymously. Land degradation refers to any reduction or loss in the biological or economic productive capacity of the land (UNCCD, 1994) caused by human activities, exacerbated by natural processes, and often magnified by the impacts of climate change and biodiversity loss. In contrast, desertification only occurs in drylands and is considered as the last stage of land degradation (Safriel, 2009).

10.3.1.2 Role of Remote Sensing for Monitoring Rangeland Degradation

Much research conducted over the last decade has been on remotely sensed biophysical indicators of land degradation processes (e.g., soil salinization, soil erosion, waterlogging, and flooding), without integration of socioeconomic indicators (Metternicht and Zinck 2003, 2009; Allbed and Kumar 2013). Studies from the 1970s onward have related soil erosion severity to variations in spectral response. Good reviews of spectrally based mapping of land degradation are found in Metternicht and Zinck (2003), Bai et al. (2008), Marini and Talbi (2009), and Shoshanya et al. (2013). Moreover, research work from the 1990s and 2000s (Metternicht. 1996; Vlek et al. 2010; Le et al., 2012; Shoshanya et al., 2013) reports the benefits of a synergistic use of satellite- and/or airborne remote sensing with ground-based observations to provide consistent, repeatable, cost-eff ctive information for land degradation studies at regional and global scales. Hereafter follows a brief description of some of the most frequent applications of remote sensing applied in "global or sub-global assessments" of land degradation. These remotely sensed products include biomass and vegetation health modeling via NDVI and NPP, rain use efficiency (RUE), and local NPP scaling.

10.3.1.3 Biomass and Vegetation Health Modeling as an Indicator of Degradation

The biomass produced by soil and other natural resources can be a proxy for land health (Nkonya et al., 2013). In this vein, Bai et al. (2008) framed land degradation in the context of the Land Degradation Assessment in Drylands (LADA) program as long-term loss of ecosystem function and productivity and used trends in 8 km^2 NDVI from the Global Inventory Modeling and

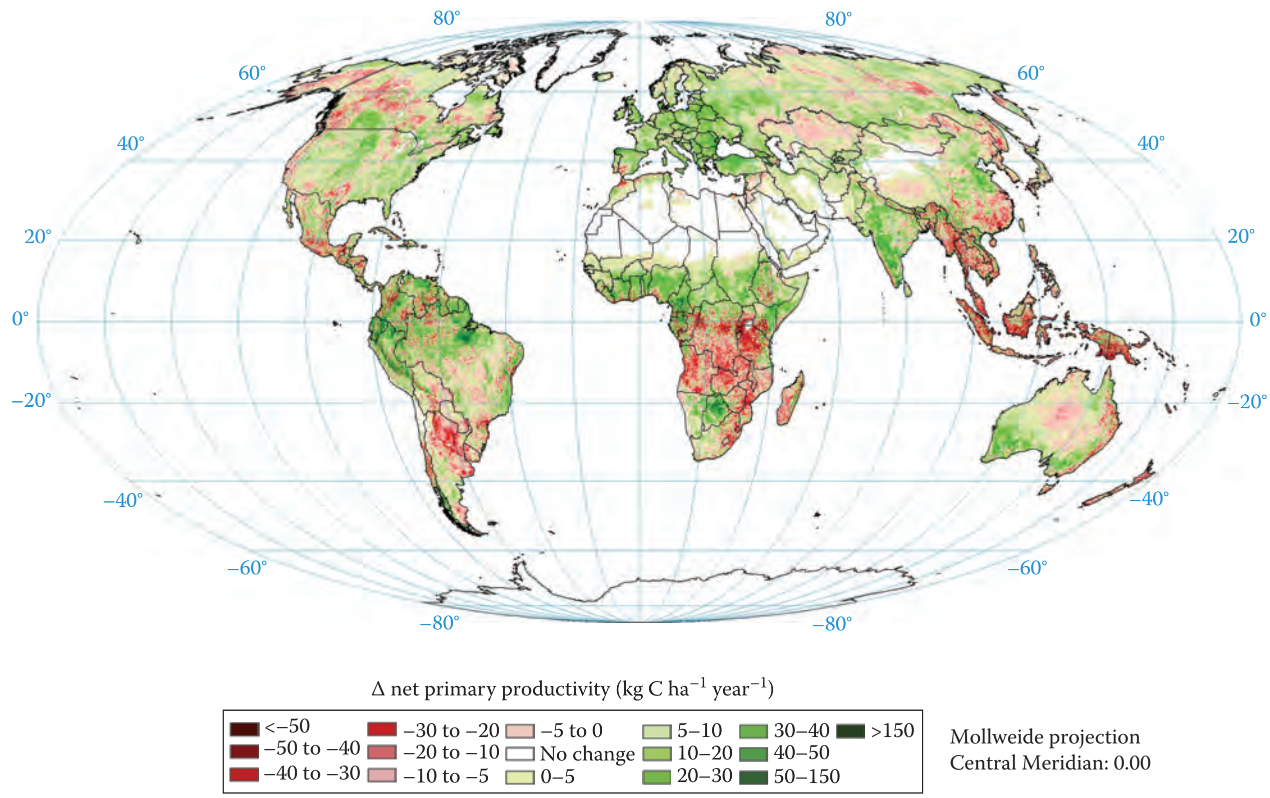

Figure 10.5 Global change in NDVI scaled in terms of NPP using MODIS 1 km^2 8-day composite net photosynthesis data (1981–2003). NDVI is a proxy indicator of changes in NPP. (From Bai, Z.G. et al., *Soil Use Manage*., 24, 223, 2008.)

Mapping Studies (GIMMS) as a "proxy indicator" of changes in NPP. Figure 10.5 represents changes in NPP from 1981 to 2003 resulting from fusion of GIMMS NDVI and MODIS 1 km^2 NPP (Bai et al., 2008). The NDVI is related to variables such as leaf area index (LAI) (Myneni et al., 1997), the fraction of photosynthetically active radiation (fPAR) absorbed by vegetation, and NPP. This explains why many NPP estimates derived from remote-sensing approaches are based on LAI, and fPAR commonly from the AVHRR onboard the National Oceanic and Atmospheric Administration (NOAA) satellite, and the MODIS on the Terra and Aqua satellites (Ito, 2011). One caveat to remotely sensed estimates of NPP for degradation analyses is the need for comparison with ground-measured biophysical parameters such as NPP, LAI, or soil erosion (or salinization) for accuracy assessment (Bai et al., 2008; Le et al., 2012).

10.3.1.4 Rain Use Efficiency

RUE (ratio of NPP to rainfall) can be used to distinguish between the relatively low NPP of drylands associated with inherent moisture deficit and the additional decline in primary production due to land degradation (Le Houérou, 1984; Le Houérou et al., 1988; Pickup, 1996). In the context of the LADA project, Bai et al. (2008) estimated RUE from the ratio of the annual sum of NDVI (derived from MODIS and NOAA AVHRR) to annual rainfall and used it to identify and isolate areas where declining productivity was a function of drought (Figure 10.6). Figure 10.6 was produced using the same GIMMS NDVI data as Figure 10.5 in concert with Variability Analyses of Surface Climate Observations (VASClimO)-gridded precipitation data at 0.5° resolution. This recalibration process was thought to yield a proxy index for land degradation, assuming that a decline in vegetation for any other reason than rainfall (and temperature) differences would be an expression of some form of degradation.

Statistical analysis showed 2% of the land area exhibited a negative trend at the 99% confidence level, 5% at the 95% confidence level, and 7.5% at the 90% confidence level (Bai et al., 2008). A drawback of this mapping approach is that an area of land degradation much smaller than 8 km^2 (pixel size of the GIMMS AVHRR) must be severe to significantly change the signal from a much larger surrounding area. In addition, the application of RUE to identify degraded landscapes has been somewhat controversial and misinterpreted as an indicator of degradation (Prince et al., 2007) since the RUE is highly variable (Fensholt and Rasmussen, 2011). In addition, errors in gridded precipitation data can add significant uncertainty, and noise to a degradation analysis suggesting analyses based solely on remotely sensed data may be beneficial (Reeves and Baggett, 2014).

10.3.1.5 Local NPP Scaling

Prince (2002) developed the local net primary productivity scaling (LNS) approach. Though the LNS approach can be applied to data of any resolution, derived from a host of sensors

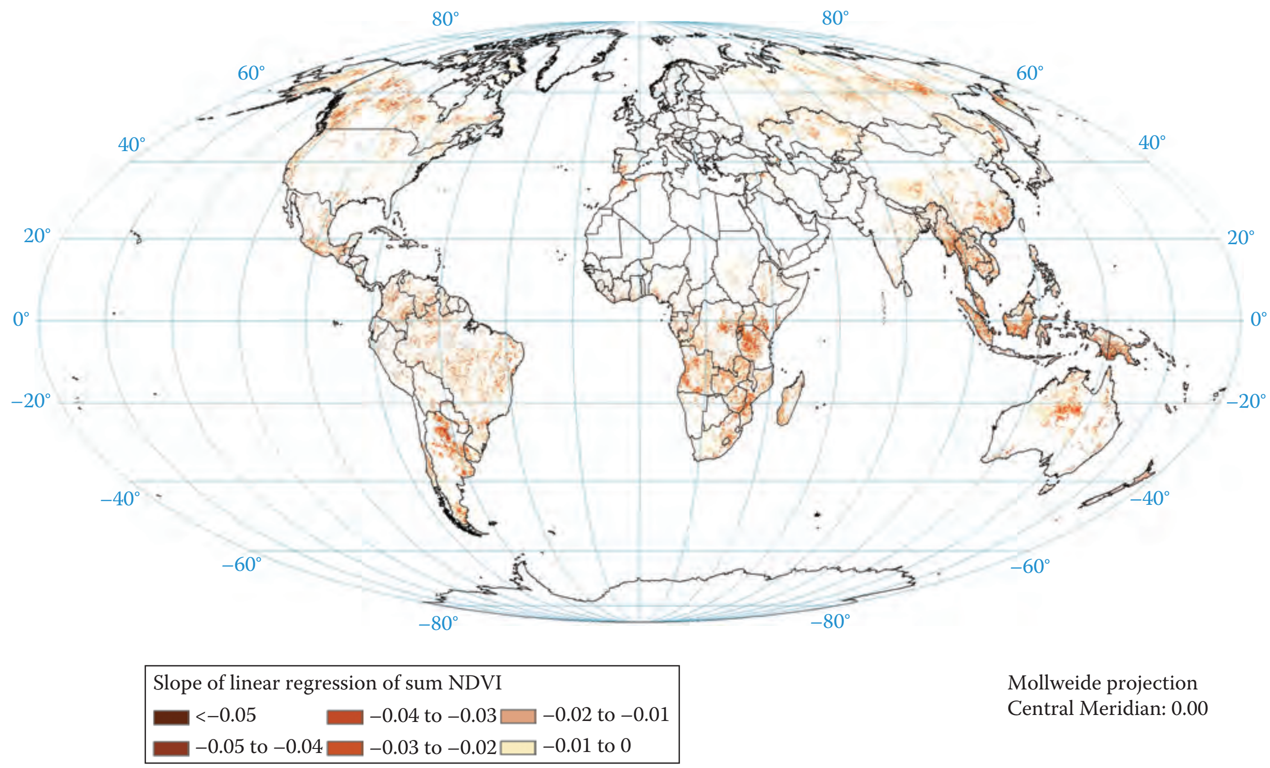

FIgure 10.6 Average RUE-adjusted NDVI, from GIMMS-AVHRR 8 km^2 and VASClimO at 0.5° spatial resolution. (From Bai, Z.G. et al., *Soil Use Manage.*, 24, 223, 2008.)

yielding visible and infrared bandpasses, AVHRR and Terra MODIS are commonly used. The LNS approach compares seasonally summed NDVI (ΣNDVI) of a single pixel to that of highest pixel value (or, commonly, the 90th percentile) observed in homogeneous biophysical land units (e.g., similar soils, climate, and landforms). The highest ΣNDVI value is assumed as a proxy for the potential aboveground NPP (ANPP) for each unit, and the other ΣNDVI values are rescaled accordingly. Prince et al. (2009) applied the LNS approach at national scales in Zimbabwe using MODIS 250 m^2 NDVI and concluded that 17.6 Tg C $year^{-1}$ were lost due to degradation. Similarly, Wessels et al. (2007) used 1 km^2 time-integrated NDVI in northeastern South Africa. More recently, Fava et al. (2012) used annual summations of MODIS 250 m^2 NDVI resolution in an LNS study for assessing pasture conditions in the Mediterranean resulting in a mean agreement of 65% with field-based classes of degradation. In a variant of the LNS approach, Reeves and Baggett (2014) used the mean 250 m^2 MODIS NDVI response of like-kind sites compared with reference conditions using a time series analysis to identify degradation on the northern and southern Great Plains, United States. With this approach, 11.5% of the region was estimated to be degraded.

10.3.1.6 Global Assessment of Land Degradation: The Evolution of Remote Sensing Use

The use of remote-sensing data in global programs of land degradation assessment is related to the history of the global assessment of human-induced soil degradation (GLASOD), the global LADA (LADA-Global Assessment of Land Degradation and Improvement [GLADA]), and the Global Land Degradation Information System (GLADIS) programs, funded by the global organizations such as United Nations Environment Program (UNEP), the UN FAO, and the Global Environmental Facility (GEF). Table 10.3 summarizes the objectives, methods, and main outputs derived from these programs, including the use of remote-sensing technologies in their implementation.

The GLASOD, an expert-opinion-based study (Table 10.3), and Oldeman et al. (1991) had two follow-up assessments, namely, the regional assessments of soil degradation status in South and Southeast Asia (Assessment of the Status of Human-induced Soil Degradation in South and Southeast Asia [ASSOD]) and Central and Eastern Europe (Soil and Terrain Vulnerability in Central and Eastern Europe [SOVEUR]) and the global LADA project, under UNEP/FAO. The LADA had the objectives of developing and testing effective methodological frameworks land degradation assessment, at global, national, and subnational scales. The global component of LADA (i.e., GLADA) provided a baseline assessment of global trends in land degradation using a range of indicators collected by processing satellite data and existing global databases (NPP, RUE, AI, rainfall variability, and erosion risk) as described in Bai et al. (2008). The GLADA was implemented between 2006 and 2009, based on 22 years (1981–2003) of fortnightly NDVI data collection and processing (Table 10.3). The project developed and validated a harmonized set of methodologies for the assessment of land use, land degradation, and

TABLE 10.3 Cursory Comparison between Major Global Rangeland Degradation Efforts

Program	Objective	Methodology—Remote Sensing Usage
Global assessment of human-induced soil degradation (GLASOD) (UNEP) (1987–1990)	Produce a world map of human-induced "soil degradation," on the basis of incomplete knowledge, in the shortest possible time	No remote sensing; expert-based approach; distinguishes "types" of soil degradation, based on perceptions; it is "not a measure" of land degradation
Land Degradation Assessment in Drylands (LADA)-GLADA—global project, under UNEP/FAO (2006–2009)	Assess (quantitative, qualitative, and georeferenced) land degradation at global, national, and subnational levels to identify status, driving forces and impacts and trends of land degradation in drylands; identify "hot" (degradation) and "bright" (improvement) spots	The global LADA was based on 22 years (1981–2003) of fortnightly NDVI data, derived from GIMMS and MODIS-related NPP (MOD 17) Method Identify degrading areas (negative trend in sum of NDVI) Eliminate false alarms of productivity decline by masking out urban areas, areas with a positive correlation between rainfall and NDVI and a positive NDVI-RUE Produce RUE-adjusted NDVI map Calculate NDVI trends for remaining areas
LADA-Global Land Degradation Information System (GLADIS) FAO-UNEP-GEF (2006–2010)	Focus on land degradation as a process resulting from pressures on a given status of the ecosystem resources	Remote sensing is used for biomass status and trends, based on a correction factor to the GLADA-RUE-adjusted NDVI, to present trends in NDVI (1981–2006) translated in greenness losses and gains distinguished by climatic and human-induced (e.g., deforestation from FAO-FRA dataset) causes. Outputs are a series of global maps on the "status and trends" of the main ecosystem services considered and radar graphs

Sources: Oldeman (1996); Bai, Z.G. et al., *Soil Use Manage.*, 24, 223, 2008; Nachtergaele et al., (2010). Prepared by Metternicht, G.

land management practices at global, national, subnational, and local levels (Ponce-Hernandez and Koohafkan, 2004).

The GLADIS was developed by FAO, UNEP, and the GEF using preexisting data and newly developed global databases to inform decision makers on all aspects of land degradation. The GLADIS developed a global land use system (LUS) classification and mapping using a set of pressures and threat indicators at the global level, allowing access to information at country, LUS, and pixel (5 arc-minute resolution) levels. It accounts for socioeconomic factors of land degradation, using a variety of ancillary data to this end. Lastly, Zika and Erb (2009) produced a global estimate of NPP losses caused by human-induced dryland degradation using existing datasets from GLASOD and other sources. Table 10.3 shows an evolution in the use of remote-sensing technology from the first global assessments (GLASOD), expert based, with no use of remote-sensing imagery, to the latest LADA-GLADIS, heavily reliant on remote-sensing derived data coupled with an ecosystem approach. The GLASOD estimated that 20% of drylands ("excluding" hyperarid areas) was affected by soil degradation. A study commissioned by the Millennium Assessment based on regional datasets ("including" hyperarid drylands) derived from literature reviews, erosion models, field assessments, and remote sensing found lower levels of land degradation in drylands, to be around 11% (although coverage was not complete) (Lepers et al., 2005). The LADA project reported that over the period of 1981–2005, 23.5% of the global land area was being degraded. On the other hand, Zika and Erb (2009) report that approximately 2% of the global terrestrial NPP is lost each year due to dryland degradation, or between 4% and 10% of the potential NPP in drylands. Figure 10.7 is a compilation of the global extent of drylands and human-induced dryland degradation, produced for the fifth Global Environment Outlook (GEO-5) based on research of Zika and Erb (2009) who express dryland degradation in croplands and grasslands as a function of NPP losses.

The three dryland area zones (top of the fi ure) are derived on basis of the AI. Only dryland areas (arid, semiarid, and dry subhumid), characterized by an AI between 0.05 and 0.65, are considered. Degradation is assessed by calculating the difference of the potential NPP (NPP_0) and current NPP (NPP_{act}). NPP losses due to human-induced degradation amount to 965 Tg C year^{-1}, giving evidence that about 4%–10% of the potential production in drylands is lost every year due to human-induced soil degradation. The largest losses are occurring in the Sahelian and Chinese arid and semiarid regions, followed by the Iranian and Middle Eastern drylands and to a lesser extent the Australian and Southern African regions (UNEP, 2012) (Table 10.4) (Figure 10.5).

A loss of NPP in the range of 20%–30% means reductions of potential productivity in that range; in most pixels of Figure 10.7, productivity losses range between 0% and 5% of their NPP_0. The results presented in Figures 10.5 and 10.7 illustrate the scope and patterns of degradation but must only be considered as rough estimates (Zika and Erb, 2009). Major uncertainties related to the results arise from three assumptions: (a) estimates of degradation extent, (b) assumptions on NPP losses due to degradation processes, and (c) potential NPP as a proxy for production potential.

In recognition of the scope of degradation globally, the UN Conference on Sustainable Development (Rio+20) prompted the international community to develop universal sustainable development goals providing a timely opportunity to respond to the threat of soil and land degradation (Koch et al., 2013). Despite over 30 years of applied research in this area, however, the need to provide a baseline and method from which to measure degradation still remains (Gilbert, 2011).

TABLE 10.4 Estimates of NPP Losses due to Dryland Degradation, Regional Breakdown

	Degraded Dryland[a]		NPP Loss[b]	
Region	1000 km^2	%	Tg C year^{-1}	%
Central Asia and Russian Federation	1,432	19.5	250	26
Eastern and Southeastern Europe	391	55.5	73	8
Eastern Asia	1,887	45.3	50	5
Latin America and the Caribbean	1,206	18.8	98	10
Northern Africa and Western Asia	1,207	33.8	70	7
Northern America	607	11.3	51	5
Oceania and Australia	866	13.2	24	2
Southeastern Asia	45	40.4	10	1
Southern Asia	1,437	30.9	106	11
Sub-Saharan Africa	2,597	22.8	215	22
Western Europe	128	24.7	18	2
Total	11,802	23.2	965	100

Source: Zika, M.E. and Erb, K.H., *Ecol. Econ.*, 69, 310, 2009.
[a] Percentage of dryland area.
[b] Estimated NPP losses associated with dryland degradation (see Zika and Erb (2009) for more detail).

For regional refinements to degradation analyses, radar satellite-based aboveground biomass estimations by Carreiras et al. (2012), or regional vegetation cover (Dong et al., 2014), could aid degradation analyses since cloud issues faced by LADA-GLADA and GLADIS could be mitigated. Additionally, Blanco et al. (2014) propose ecological site classification of semiarid rangelands enabling more refined spatial units across which remote sensing can be conducted. Finally, engaging citizens in knowledge production (including field verification of remotely sensed derived information), as fostered by current global (UNEPLive, Future Earth, Group on Earth Observations Biodiversity Observation Network) and subglobal initiatives (Eionet of the European Environmental Agency), could address the significant lack of ground truthing of previous global land degradation studies.

10.3.2 Fire in Global Rangeland Ecosystems

The extremely wide range of rangeland environments makes it virtually impossible to develop generalized statements about global fire regimes. However, the general composition of fuel and fuel characteristics defines some specifics of fire occurrence common for these ecosystems. Vegetation of rangelands

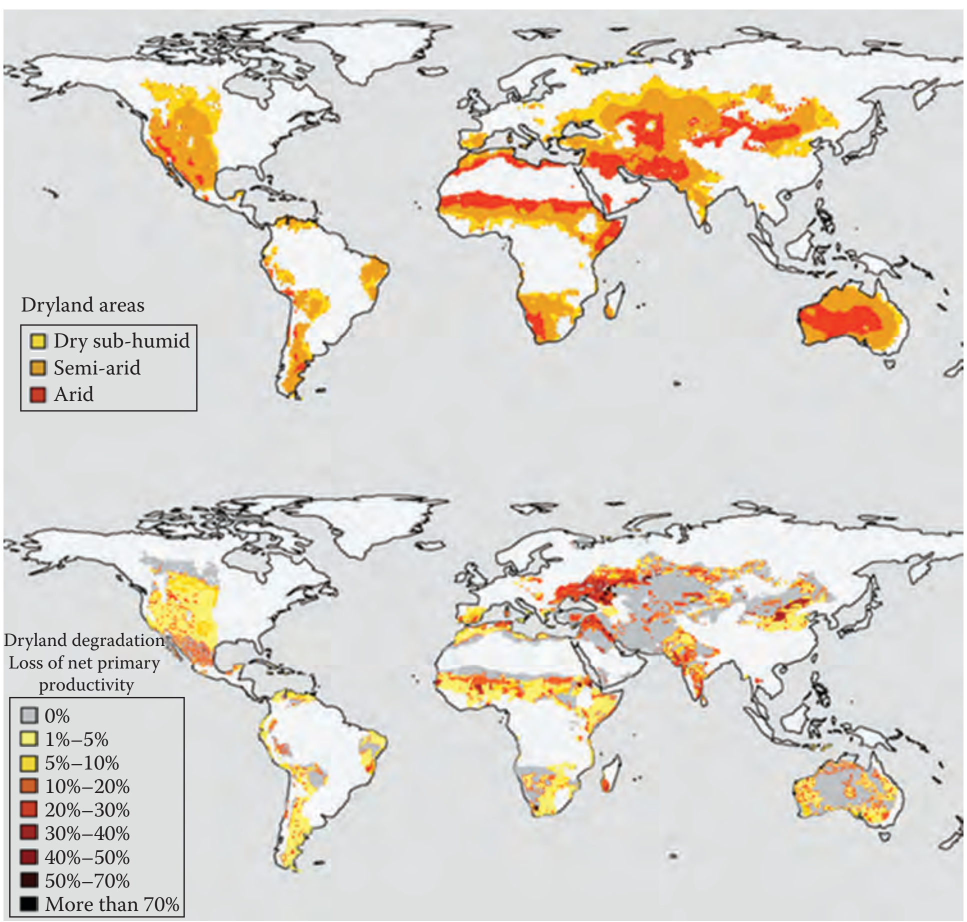

FIGURE 10.7 Global extent of drylands and human-induced dryland degradation. (From UNEP, 2012. Redrawn from Zika, M.E. and Erb, K.H., *Ecol. Econom.*, 69, 310, 2009; We thank UNEP and the GEO-5 process for use of the figure.)

is characterized by fast growth and slow decomposition rates (Vogl, 1979) leading to considerable buildup of surface litter. The majority of fuels in these ecosystems, with the possible exception of chaparral systems, are flash and fine fuels (<0.25 in diameter), which dry out rapidly (i.e., 1-h time lag fuels) and burn readily (National Wildfire Coordinating Group, 2012). Therefore, it is not unusual for these ecosystems to transition from low-fire danger state to extreme-fire danger state over a comparatively short period. Contiguity and loading of fuel in these ecosystems is highly variable both spatially and temporally: interannual variation in fuel loading often exceeds 110% (Ludwig, 1987). While fire is currently a common and widespread disturbance agent globally in rangelands, its prominence is expected to rise under projected climate change. Past and ongoing satellite monitoring and mapping of rangeland fire extent provide a much needed baseline for assessment of potential future change in fire occurrence and its impact on ecosystem functioning.

10.3.2.1 Satellite Monitoring of Ongoing Burning

The hotspot detections from the nighttime top of atmosphere radiance data from the Along-Track Scanning Radiometer (ATSR-2) and Advanced ATSR (AATSR) were used to build the first World Fire Atlas (Jenkins et al., 1997). Neither of the source instruments was designed to support fire detection specifically, and therefore, the algorithms were based on suboptimal ranges of electromagnetic radiation (at brightness temperature [BT] centered on 3.7 and 11.8 μm) using a suite of simple thresholds (Arino et al., 2012). The MODIS was, however, designed with a specific goal to enhance fire-mapping capabilities (Kaufman et al., 1998). MODIS collects daily global observations from Terra ~11:30 a.m. and 11:30 p.m. and Aqua at ~1:30 a.m. and 1:30 p.m. equatorial crossing time. In addition, several “fire” channels were included in the instrument to support fire monitoring: two 4 μm channels (channel 21 with 500 K saturation level and channel 22 with 331 K saturation level) and 11 μm channel (channel 31 with 400 K saturation level) at 1 km^2 nominal resolution (Giglio et al., 2003). The flexibility of switching the high- and low-saturation 4 μm channels in the contextual active fire detection algorithm is particularly important for tropical savanna environments.

The MODIS active fire product is the first product to include fire characterization metrics in addition to the binary “fire/no fire” masks. Fire radiative power (FRP), expressed in watts (W) is an instantaneous measurement of power released by ongoing burning during the satellite overpass (Kaufman et al., 1996a,b) and are estimated using an empirical relationship established in Kaufman et al. (1998). FRP is directly related to the intensity of biomass burning and, when integrated overtime to fire radiative energy (FRE) expressed in joules (J), is linearly related to biomass consumption (Wooster et al., 2005).

10.3.2.2 Satellite Estimates of Burned Area

Unlike active fire detection, which is primarily based on BT in mid- and long-infrared spectrum, burned area estimates are most frequently based on changes in surface reflectance due to burning observable within the visible (0.4–0.6 μm), NIR (0.7–1.0 μm), and shortwave infrared (SWIR 1.1–2.4 μm) spectrum. The relatively short wavelength of radiation in this range determines that burned area mapping relies on clear-surface observations and is strongly limited by considerable aerosol contamination from smoke during the burning process and high cloud cover in high northern latitudes.

The first multiyear global burned area products were developed from data acquired by VEGETATION (VGT) (onboard SPOT), ATSR-2 (onboard ERS-2), Medium Resolution Imaging Spectrometer (MERIS), and AATSR (onboard Environmental Satellite [ENVISAT]) instruments (Plummer et al., 2006) within the GLOBCARBON initiative. The suite of fire products developed from the MODIS 500 m^2 data includes two global burned area algorithms. The MCD45 algorithm (Roy et al., 2008) is based on detection of rapid changes in surface reflectance within a MODIS 500 m^2 pixel (Figure 10.8).

The MCD64 algorithm (Giglio et al., 2009) relies on detection of persistent changes in vegetation state and subsequent attribution of the change to burning by comparison to active fire occurrence within a specified spatiotemporal window. A detailed study in Central Asia (Loboda et al., 2012) has shown that MODIS-based products deliver spatially accurate estimates of burned area in Central Asia. However, MCD45 on average underestimates the total amount of burned area by ~30%, whereas MCD64 estimates are considerably closer to Landsat-based assessments (~18% underestimation). The independent accuracy assessment results within drylands of Central Asia are similar to those in North America (Giglio et al., 2009). This makes MODIS-based products appear to deliver a reasonable estimate of fire impact on grasslands and shrublands of the world.

10.3.2.3 Remote-Sensing Methods for Fire Impact Characterization

The large footprint of savanna fires, remote locations of tundra fires, and overall short longevity of scars of grass- and shrub-dominated fires make remote sensing the only viable source of data for consistent global postfire characterization of burned area. While a healthy debate about what constitutes burn severity and how much the ecological definition ranges across ecosystems is still ongoing in the fire science community (French et al., 2008), the Monitoring Trends in Burn Severity (MTBS) program established the baseline definition. This includes the assumption that this parameter can be mapped from remotely sensed data and is ultimately based on a combination of “visible changes in living and nonliving biomass, fire byproducts (scorch, char, and ash), and soil exposure” among other components (Eidenshink et al., 2007). The same ranges of electromagnetic spectrum (visible–NIR–SWIR), therefore, constitute the basis for the strongest differentiation between soil, vegetation, char, and ash components characterizing burn severity as those used most commonly for burned area mapping. It is not surprising that the first widely applied index for mapping and quantifying burn severity is based on the normalized difference of NIR and SWIR in 2.2 μm range ($SWIR_{2.2}$) originally developed by Lopez-Garcia and Caselles (1991) for burned area mapping. The Normalized

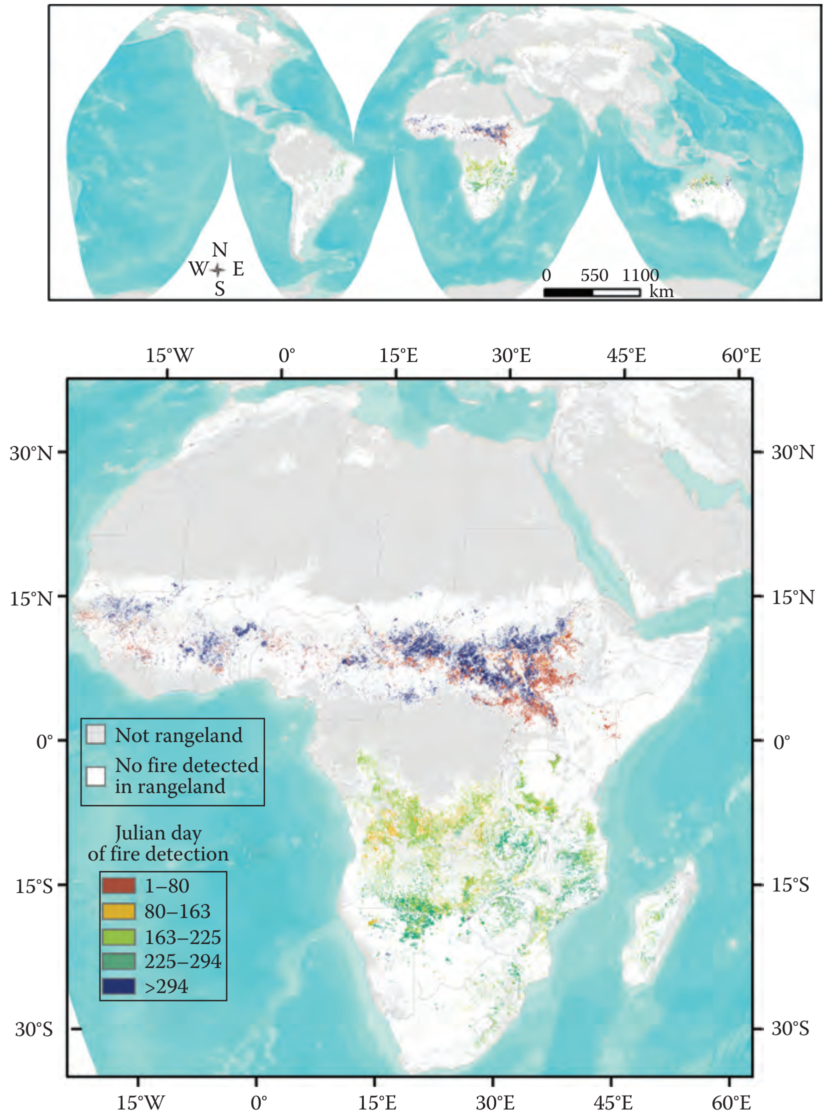

FIGURE 10.8 Example of the MCD45 MODIS product for depicting approximate date of fire in rangelands globally. (Prepared by Matt Reeves. MCD45 MODIS data for 2013.)

Difference Burn index (NDBR), as it was subsequently named by Key and Benson (1999a,b), is calculated as follows:

$$\mathrm{NBR} = \frac{\mathrm{NIR} - \mathrm{SWIR}_{2.2}}{\mathrm{NIR} + \mathrm{SWIR}_{2.2}}$$

where

NIR refers to the TM band 4 (0.76–0.90 μm)
$\mathrm{SWIR}_{2.2}$ refers to band 7 (2.08–2.35 μm)

Key and Benson (1999a,b) aimed to capture the fire-induced changes to the proportions of soil, char, ash, and vegetation through differencing the preburn and postburn NDBR measurement within a fire perimeter. This approach (differenced normalized burn ratio [dNBR], calculated as dNBR = $\mathrm{NBR}_{\text{pre-burn}} - \mathrm{NBR}_{\text{post-burn}}$) has become the most widely applied metric of burn severity across all ecosystems in the United States (Eidenshink et al., 2007).

Compared to forest cover, where the original assessment of dNBR were closely related to field measurements of burn severity expressed through a composite burn index (CBI) (Key and Benson, 2006, Allen and Sorbel, 2008), these grass- and shrub-dominated ecosystems have a low amount of aboveground biomass and are spatially highly heterogeneous. Thus, the magnitude of change between preburn and postburn surface conditions is considerably more muted and uneven. To account for the initial lower fuel loading in these ecosystems, an adjustment to dNBR, named relativized dNBR (RdNBR), was developed by Miller and Thode (2007). This index is calculated as follows:

$$\mathrm{RdNBR} = \frac{\mathrm{dNBR}}{\sqrt{\left|\mathrm{NBR}_{\text{pre-burn}}/1100\right|}}$$

Although RdNBR versus CBI assessments show that RdNBR is more robust in assessing burn severity compared to dNBR in grass- and shrub-dominated ecosystems (Miller and Thode, 2007; Loboda et al., 2013), it does not overcome a major limitation of spectral signature change due to fire in NIR/SWIR spectral space within these ecosystems.

It is likely that the success rate of any one spectral index in mapping and quantifying burn severity depends strongly on the specific proportions of grass, woody biomass, exposed soil, geographic location (as related to frequency of observation allowing for a wider range of mapping days and different sun-sensor geometries), moisture status during image acquisition, and the timing of mapping.

10.3.3 Food Security: Role of Remote Sensing in Forage Assessment

On rangelands, quantifying the amount of forage available to livestock on a near real-time basis using traditional methods (e.g., clipping vegetation along transects) can be costly, time consuming, and logistically challenging. A lack of information for making livestock management decisions at critical times could lead to loss of livestock due to lack of forage, or lead to vegetation overuse, which, in turn, could result in rangeland degradation (Weber et al., 2000). Therefore, having an objective means of setting stocking rates on rangelands based on productivity will allow rangeland managers to better adapt to changing weather conditions.

Because of the large areal cover that remote-sensing products provide, in addition to the greater temporal frequencies of collection compared to traditional field sampling over large areas, the use of remote-sensing imagery is attractive for assessing vegetation production on rangelands. Multiple satellite platforms exist that are useful for rangeland forage assessments and early warning systems. Two approaches have generally been used for assessing rangeland forage conditions using remote-sensing imagery. These include (1) empirical approaches that estimate the forage biomass or quality based on a statistical relationship between the spectral bands (or some combination of bands) in the imagery and field-collected vegetation data and (2) process models that use remote-sensing data as inputs for predicting vegetation biomass or quality.

10.3.3.1 Empirical Approaches

Empirical approaches for assessing rangeland forage conditions using remote-sensing products generally involve the use of a statistical relationship between the remote-sensing spectral response or product variable and data collected from field measurements (Dungan, 1998). Using the empirical approach example in Figure 10.9, a MODIS 250 m^2 maximum value composite and NDVI value of 7500 correspond to approximately 3414 kg ha^{-1} of annual production, after accounting for unavailability ($\phi = 0.15$) and suggested utilization ($\upsilon = 0.5$) results in stocking rate of 5.3 animal unit month's (AUM) ha^{-1}.

In a similar manner, Tucker et al. (1983) used both a linear and logarithmic regression between the ground-collected biomass data in the Sahel region and AVHRR NDVI to predict biomass on a regional scale. Al-Bakri and Taylor (2003) used a linear regression approach to predict shrub biomass production for

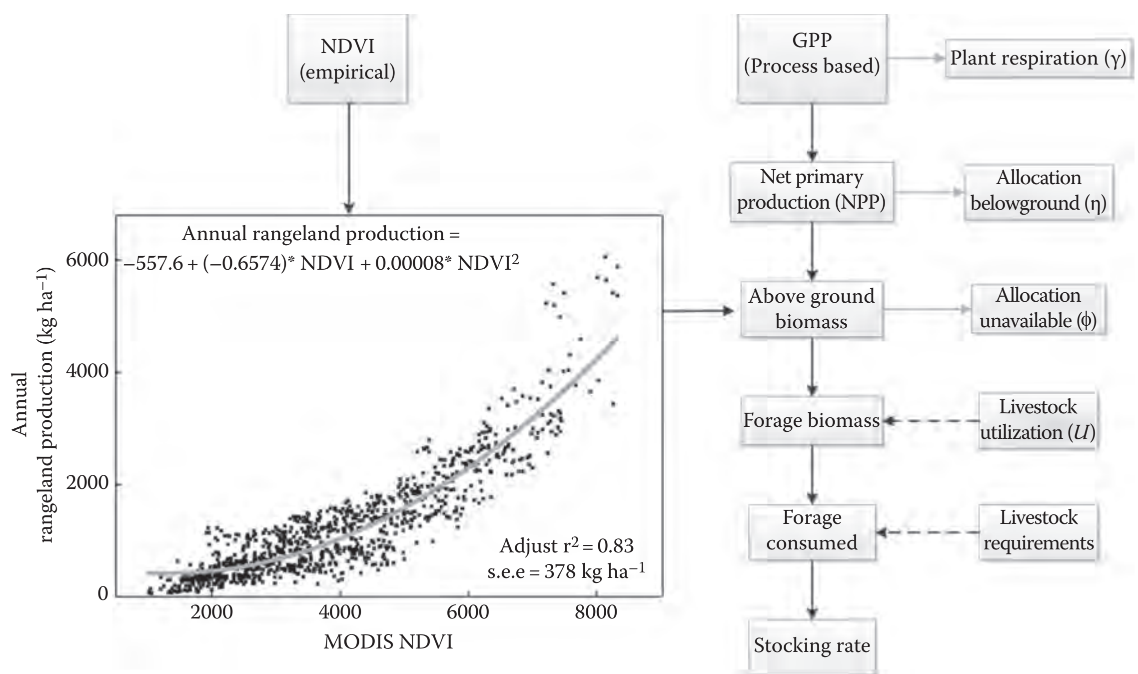

FIGURE 10.9 Process for estimating stocking rate from remote-sensing data, either empirically or using a process model. GPP is determined from land cover type, spectral vegetation indices, incident photosynthetically active radiation, and climate-dependent radiation use efficiencies or empirically. Solid arrows represent reductions based on physiology, while dashed arrows represent critical management decisions are determined.

rangelands in Jordan using 7.6 km^2 AVHRR NDVI. Both these studies reported accounting for >60% of the variation in herbaceous biomass with AVHRR NDVI alone using linear regression against biomass. In the Xilingol steppe of Inner Mongolia, Kawamura et al. (2005) used 500 m^2 MODIS enhanced vegetation index (EVI) to predict live biomass and total biomass of livestock forage with linear regression models, which accounted for 80% of the variation in live biomass and 77% of the variation in total biomass. In the Tibetan Autonomous Prefecture of Golog, Qinghai, China, Yu et al. (2011) used the 250 m^2 resolution MODIS NDVI to estimate aboveground green biomass using regression relationships between the NDVI and field-collected biomass data (r^2 of 0.51) from sites across the region.

As with forage biomass, empirical approaches can be used for forage quality assessments generally involving examining statistical relationships between forage quality variables such as crude protein or energy and spectral information from remote-sensing imagery. For example, Thoma et al. (2002) used simple linear regression with AVHRR NDVI as the independent variable to predict forage quality and quantity on rangelands in Montana, United States. Their analysis indicated reasonable relationships between NDVI and live biomass (r^2 = 0.68) and nitrogen in standing biomass (r^2 = 0.66). Similarly, Kawamura et al. (2005) used regression relationships between field-collected data and MODIS EVI to predict live and dead biomass and crude protein in standing biomass. They found good predictability between standing live biomass and total biomass (live + dead) (r^2 = 0.77–0.80), but correlations with crude protein were poor (r^2 = 0.11).

Remote-sensing imagery provides a dense and exhaustive dataset that can serve as a secondary variable for geostatistical interpolation given that a correlation exists (both direct and spatial) between the primary and secondary variable (Dungan, 1998). Use of MODIS NDVI in the cokriging analysis of forage crude protein provides reasonable during the dry season (r^2 = 0.69) but less so during the wet season (r^2 = 0.51) (Awuma et al., 2007) likely because the amount of unpalatable shrub cover increased the greenness signal in the NDVI in some of the sampling areas that did not contribute to the available forage.

10.3.3.2 Process Models Using Remote-Sensing Inputs

One problem that has been noted for regression models that use remote-sensing variables is that they violate the regression assumption of no autocorrelation in the predictor variable(s) (Dungan, 1998; Foody, 2003). Since most remote-sensing data are inherently autocorrelated, violation of this assumption may reduce the effectiveness of the regression model (Dungan, 1998). One way of overcoming the autocorrelation problems is to use process models that are driven by remotely sensed input variables on a pixel-by-pixel basis. Reeves et al. (2001) describe such an approach for predicting rangeland biomass using remote-sensing products from the MODIS system and a light use efficiency model for plant growth. Hunt and Miyake (2006) used a similar light use efficiency model approach for estimating stocking rates for livestock at 1 km^2 resolution in Wyoming, United States (Figure 10.9). Using the approach of Hunt and Miyake (2006), the stocking rate is estimated as gross primary production (GPP) $(1 - \chi)(1 - \eta)(1 - \phi)\ \upsilon$ (AUM/273 kg month^{-1}). From Hunt and Miyake (2006), the parameters for grasslands are approximately $\chi = 0.48$, $\eta = 0.79$, $\phi = 0.15$, and $\upsilon = 0.5$ where χ is autotrophic respiration, η is belowground carbon allocation, ϕ is carbon allocation to nonpalatable stems and other vegetation, and υ is an estimated accepted level of utilization. Therefore, a monthly GPP of 11,000 kg ha^{-1} month^{-1} is about 1.7 AUM's ha^{-1}, but this is just one method of using process models parameterized with remote-sensing inputs.

An example of a process-based modeling approach for forage quantity assessment at the regional level is the Livestock Early Warning Systems (LEWS) in East Africa (Stuth et al., 2003a, 2005) and Mongolia (Angerer, 2012) (Figure 10.10).

Figure 10.10 presents results of the LEWS applied in Mongolia in 2013. Note the significant decline of forage in southwestern Mongolia in 2013. The LEWS was developed to provide near real-time estimates of forage biomass and deviation from average conditions (anomalies) to provide pastoralists, policy makers, and other stakeholders with information on emerging forage conditions to improve risk management decision making. The LEWS combines MODIS 250 m^2 NDVI, field data collection from a series of monitoring sites, simulation model outputs, and statistical forecasting, to produce regional maps of current and forecast forage conditions and anomalies. The system uses the Phytomass Growth Simulation model (PHYGROW) (Stuth et al., 2003b), parameterized with the MODIS 250 m^2 NDVI, as the primary tool for estimating available forage. Model verification indicates the model performs well in estimating forage biomass (Stuth et al., 2005). For example, model verification across monitoring sites in Mongolia indicated a good correspondence between the PHYGROW predicted biomass and observed field data (r^2 = 0.76) with forage biomass ranging from 3 to 1230 kg ha^{-1}. PHYGROW had a tendency to underestimate forage biomass across sites by 14% with an overall mean bias error of −18 kg ha^{-1} (Angerer, 2008).

10.3.4 Rangeland Vegetation Response to Global Change: The Role of Remote Sensing

Monitoring global change is an increasingly important endeavor (Running et al., 1999) since ecosystem goods and services, essential to human survival, are directly linked to the health of the biosphere (Fox et al., 2009). The Earth is a dynamic system with many interacting components that are complex and highly variable in space and time. Though change has always been present, human activities have influenced rates and extent of change beyond historical ranges (Vitousek, 1992; Levitus et al., 2000; Foley et al., 2005). Global change involves terrestrial, aquatic, oceanic, and atmospheric systems and cycles and is not limited to climate change alone (Beatriz and Valladares, 2008). Other factors such as invasive species, habitat change, overexploitation,

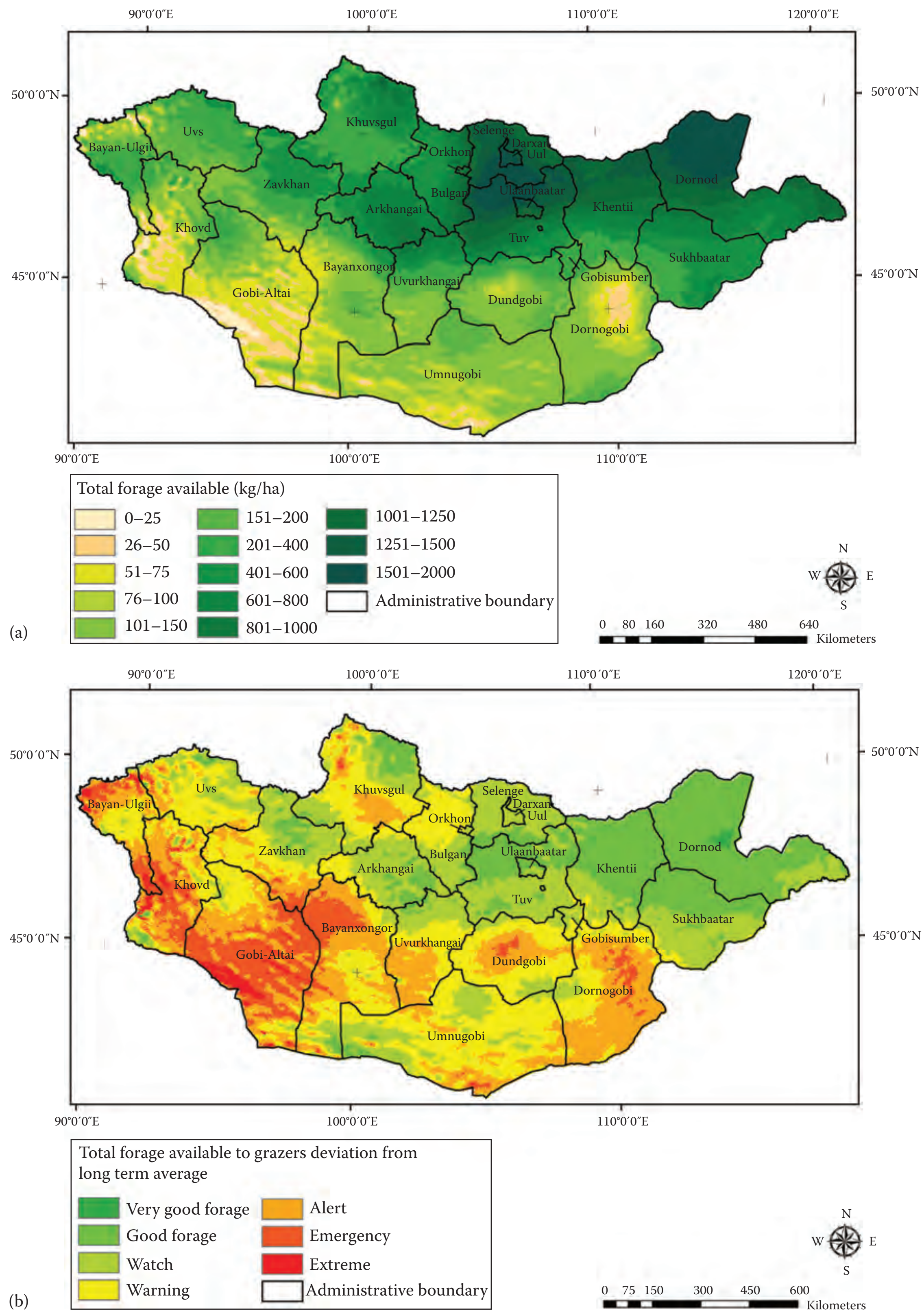

FIGURE 10.10 Panel (a) represents total forage available (kg ha^{-1}) during August 2013 for the Mongolia LEWS. Panel (b) represents a map of forage deviation from long-term average (i.e., forage anomaly) for August 2013. Note areas in southwestern Mongolia experiencing emergency to extreme drought conditions.

and pollution are equally or even more important to the Earth's future (Millennium Ecosystem Assessment, 2005). Thus, the goal of global monitoring is aimed at characterizing "human habitability" through evaluation of vegetation that provides food, fiber, and fuel (Running et al., 1999) to a rapidly growing population. In the burgeoning field of global change monitoring, satellite remote sensing is increasingly more important. Only remote sensing offers a truly synoptic perspective of our surroundings and is therefore a critical tool for describing the type, rate, and extent of change unfolding across the globe. This is especially true for rangeland ecosystems that experienced losses of about 700 million ha by 1983 due to agriculture. In the United States alone, an estimated 75 million ha of former rangelands have been converted to agricultural land use since Euro-American settlement (Reeves and Mitchell, 2011) (Figure 10.11). The impacts of global change, such as climate impacts and land conversion, are often quantified through evaluation of vegetation cover and NPP in the context of the global carbon budget (Running et al., 1999).

10.3.4.1 Vegetation Productivity

Given the lack of field-referenced data available for determining productivity for rangelands globally, ecosystem modeling, remote sensing (Hunt and Miyake, 2006; Fensholt et al., 2006; Reeves et al., 2006), or a combination of both (Jinguo et al., 2006; Wylie et al., 2007; Xiao et al., 2008) can be used to estimate spatial and temporal trends across large areas. Many studies have evaluated the growth, total production, and health of rangeland vegetation, but two general approaches are normally applied that are very similar to the procedures outlined in the food security section. The first approach involves directly sensing, via radiometric measurement, the amount of growth that has occurred over a given time period.

Direct quantification of biomass across rangeland vegetation types requires a set of spatially explicit field samples describing

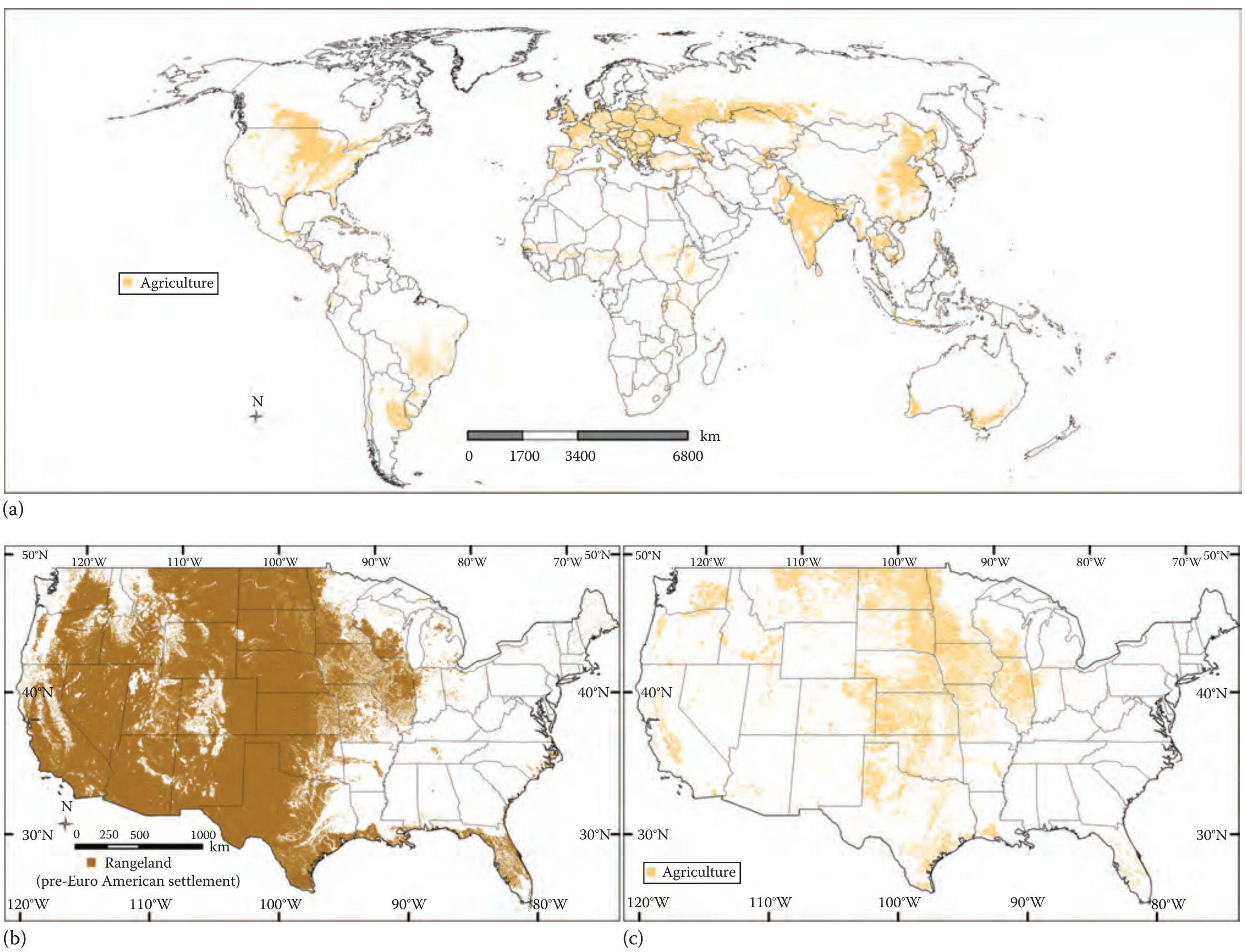

FIgure 10.11 Panel (a) represents the estimated distribution of agricultural land use globally derived from MODIS MOD12Q1, 2006; University of Maryland Classification. Also shown is the hypothesized pre-Euro-American extent of rangeland (From Reeves, M.C. and Mitchell, J.E., *Rangeland Ecol. Manage.*, 64, 1, 2011.) as is shown in Panel (b), while Panel (c) demonstrates areas of former rangeland now in agricultural production (estimated using the Biophysical Settings data product from the Landfire Project; Rollins, 2009).

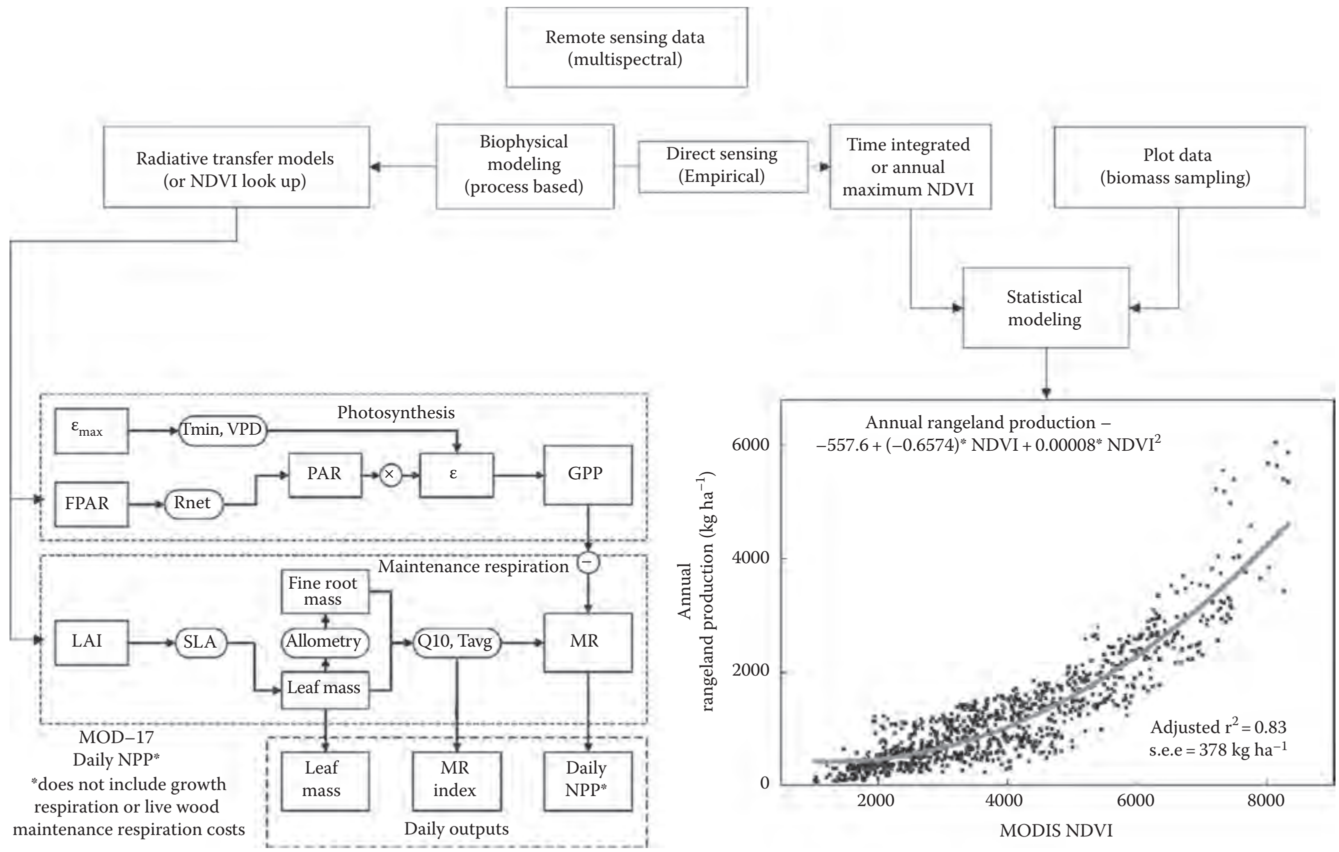

FIgure 10.12 Direct sensing and biophysical modeling (process modeling) are two methods for estimating productivity of rangeland landscapes.

the amount of peak biomass or annual production. Once field data are collected and properly scaled, statistical models can be developed to describe the relationship between NDVI and biomass (Figure 10.12) that can, in turn, be used to monitor the response of vegetation through time. If peak biomass is estimates are sought, the annual maximum NDVI value should work reasonably well, but if annual production estimates are desired, a time integration of NDVI is usually employed (e.g., Paruelo et al., 1997).

Though NDVI has been widely used for monitoring global vegetation conditions, it exhibits well-known saturation characteristics at relatively higher levels of biomass. The EVI can be used, with some success to overcome the saturation limitations inherent in NDVI. The saturation component of the NDVI signal, however, does not render it less useful for most applications. The reason for this is that across the range of productivity levels expected in most rangeland environments, the response is linear (Skidmore and Ferwerda, 2008).

The second approach for monitoring growth, total production, and health of vegetation involves use of remote sensing for quantifying canopy parameters, such as LAI, and fPAR, which, in turn, become part of a vegetation modeling system (Figure 10.12). Such a system is exemplified by the MODIS NPP algorithm (MOD17), which provides gross and NPP products at 1 km^2 resolution for the entire globe. This approach is more sophisticated than direct sensing of biomass but enables carbon accounting for the global extent of rangelands. The modeling approach also requires a good deal more information including biome specific physiological parameters (Running et al., 2004). In addition, since this type of modeling approach requires meteorological and land cover information, it is directly informed by land cover/land use changes associated with global change. The NPP of rangeland vegetation from 2000 to 2012 is depicted in Figure 10.13, which demonstrates the type of ecosystem analysis possible with the MODIS NPP product.

Figure 10.13 was created using a time series analysis from 2000 to 2012 of the MODIS-derived annual NPP and Collection 4.5 land cover products. From this analysis, significant overlap and similarities between the savanna and woody savanna land cover classes are evident. These similarities suggest similar biophysical and bioclimatic conditions are present in these two classes or confusion exists between the classes. The close relationship between woody savanna and savanna could also be related to spatial commingling of the two types, which could be alleviated using higher-resolution imagery. Multisensor fusion between MODIS (high temporal resolution) and Landsat (e.g., ETM+—high spatial resolution) can be used to explore why woody savannas and savannas are performing very similarly.

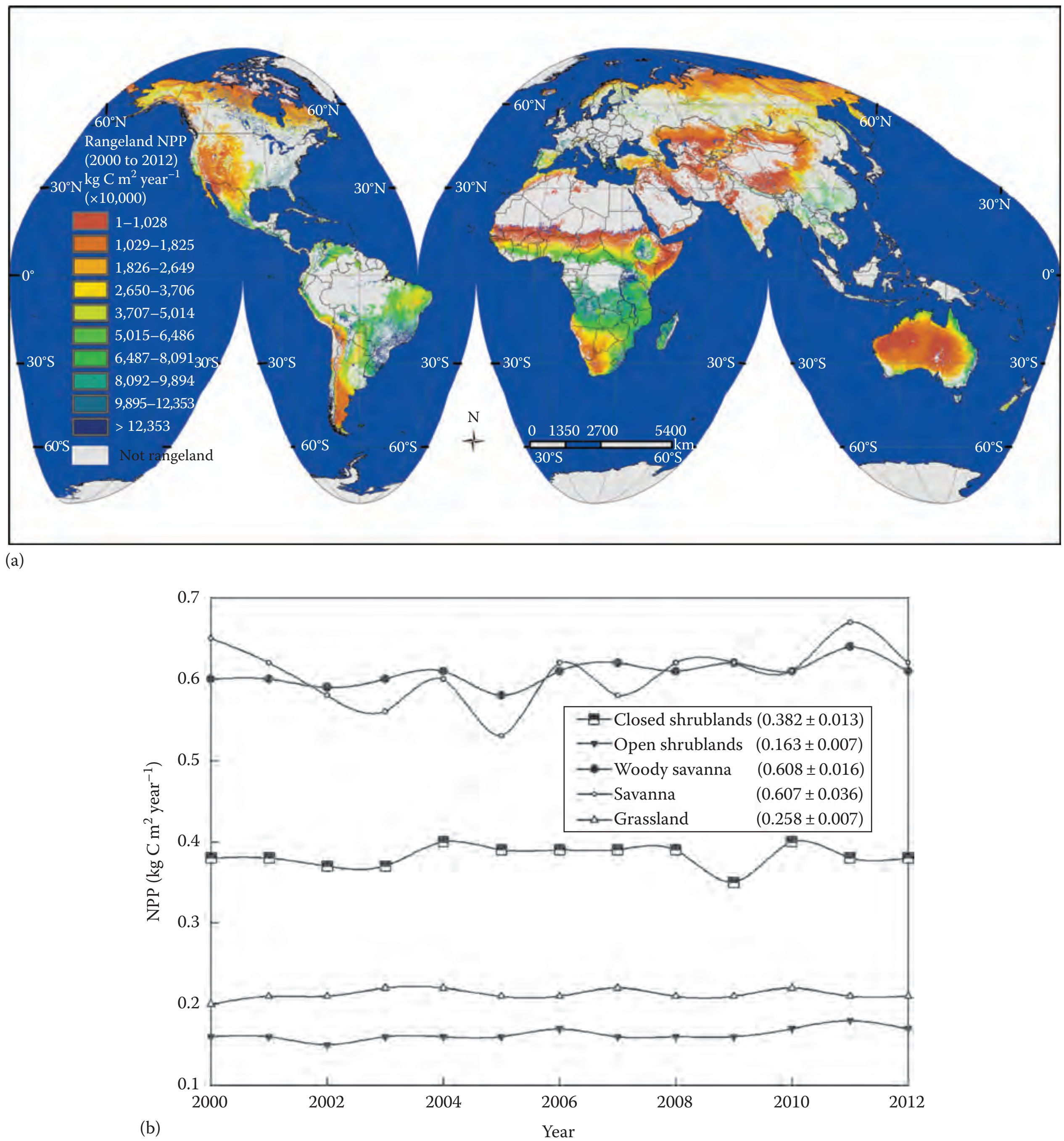

FIGURE 10.13 Panel (a) represents the mean (2000–2012) global distribution of rangeland NPP from the MODIS NPP (MOD17) product. Panel (b) represents the time series (2000–2012) of global rangeland NPP from the MOD17 product.

Roy et al. (2008) used MODIS 500 m^2 bidirectional reflectance distribution function spectral model parameters and the sun-sensor geometry to estimate ETM surface reflectance to fill temporal gaps between suitable ETM+ overpasses. This process resulted in prediction errors in the NIR dataspace of about 12% overall. Directly incorporating effects from changing climate, land cover, and associated vegetation responses simultaneously enables improved analysis of global change effects on rangeland environments. One major goal of satellite remote sensing is observation of vegetation over large areas and for long periods of time. The appropriate length of observation depends on the behavior of the phenomena to be studied. Developing long-term observations requires much effort to ensure continuity across new sensors with varying bandpasses and associated target-atmospheric effects, drifts in calibration, and filter degradation (Huete et al., 2002).

10.3.4.2 Extending Remote Sensing Time Series Using Cross-Sensor Calibration

Recent ecological research has shown that declines in dryland productivity (often estimated measured using trends in NDVI and/or NPP), and increases in soil loss are due to the synergistic effects of extreme climatic events and land management practices. In particular, livestock grazing and El Niño and La Niña events have 3- to 7-year return intervals (Holmgren and Scheffer, 2001; Holmgren et al., 2006; Washington-Allen et al., 2006) indicating that 10–20 years of continuous data is required to replicate, monitor, and assess the influence of land use practices and these extreme events (Washington-Allen et al., 2006).

Sensors have finite life spans, and developing long-term observations often requires using multiple sources of data to develop a continuous, compatible dataset. The extension of time series is challenging due to drifts in calibration, filter degradation, and band locations (Miura et al., 2006). These characteristics create errors and uncertainties that vary with the landscape and sensors being evaluated. As examples, red and NIR spectral channels from AVHRR are relatively broad occupying the spectral space between 580–680 and 730–1000 nm, respectively. In contrast, MODIS provides more narrow bands in the red and NIR space at 620–670 and 841–876 nm, respectively. The broader AVHRR red channel incorporates a portion of the green reflectance region (500–600 nm) (Figure 10.4) inevitably yielding a different spectral response of vegetation than MODIS.

The approaches for extending a satellite data time series via sensor (or product) cross-calibration involve remote-sensing data fusion that accounts for multisensory, multitemporal, multiresolution, and multifrequency image data from operational satellites (Pohl and Van Gederen, 1998; Zhang et al., 2010). Extension of satellite data records to produce time series of NDVI or NPP data typically involve

1. Development of equations to simulate the spectral responses of individual channels (e.g., Suits et al., 1988)
2. Development of calibration equations to simulate the vegetation indices derived from other sensors (e.g., Steven et al., 2003; Tucker et al., 2005)
3. Cross-calibration of NDVI (e.g., from AVHRR) and NPP data products (e.g., from the MODIS sensor) to back cast the NPP record

These techniques have been explored in a good number of studies and indicate suitable relations between sensors, but results are often inconclusive (Fensholt et al., 2009). Suits et al. (1988) determined that multiple regression analysis compared to principle component analysis was the best approach for spectral response substitution between Landsat and AVHRR sensors. Steven et al. (2003) found that vegetation indices from Landsat, SPOT, AVHRR, and MODIS were strongly linearly related, which allowed them to develop a table of conversion coefficients that allowed simulation of NDVI and SAVI across these sensors within a 1%–2% margin of error. With the exception of AVHRR, which was designed for other purposes, most high temporal resolution sensors have similar sensitivity to green vegetation. In addition, vegetation indices from many global platforms can be calibrated to within approximately ±0.02 units if surface reflectance (as opposed to top of atmosphere) is used (Steven et al., 2003). Fensholt and Proud (2012) compared the GIMMS 3g 8 km^2 NDVI archive with MODIS 1 km^2 NDVI and showed that global trends exhibit similar tendencies but significant local and regional differences were present, especially in more xeric environments. A comprehensive analysis of four long-term AVHRR-based NDVI datasets with MODIS and SPOT NDVI datasets for the common period (from 2001 to 2008) clearly demonstrated lower correlations in more xeric regions such as the southwest and Great Basin of the United States (Scheftic et al., 2014). Similarly, Gallo et al. (2005) reported that 90% of the variation between 1 km^2 MODIS and AVHRR NDVI can be explained by a simple linear relationship, while Miura et al. (2006) developed translation equations to emulate MODIS NDVI from AVHRR resulting in an r^2 of 0.97. Despite these successes, trend analyses from AVHRR can differ strongly from those estimated with MODIS and SPOT-VGT (Steven et al., 2003) and lead to spurious conclusions. Unlike MODIS, AVHRR does not provide additional necessary channels permitting analysis of atmospheric composition for suitable atmospheric correction (Yin et al., 2012). Therefore, cross-sensor calibration must be carefully planned and should leverage the strengths of previous efforts. Most efforts aimed for extending time series to improve trend analyses involve spectral calibration, either of individual band passes or indices. For monitoring global change and ecosystem performance, however, it is useful to quantify NPP trends given its link with the global carbon cycle and paramount importance to maintaining goods and services. Bai et al. (2008, 2009) developed a 23-year time series of global NPP data from 1982 to 2003 using the overlap period (2000–2003) between 1 km^2 MODIS NPP and the mean annual sum of 8 km^2 AVHRR GIMMS, for LADA program of FAO. Next, linear regression was applied to 4-year mean, global, annual sum of NDVI from the GIMMS dataset and MODIS NPP to generate a single empirical equation between these two datasets. The resulting equation was then used to produce an 8 km^2 NPP time series from 1982 to 2003. Wessels (2009) critiqued the approach of Bai et al. (2008) arguing that spatial variability was reduced and unaccounted for by using a single mean equation rather than a pixel-by-pixel approach. As a result, the following case study used a pixel-wise regression approach for establishing relationships between 8 km^2 GIMMS NDVI and 1 km^2 MODIS NPP. The goal of this case study was to produce a continuous, compatible dataset describing annual NPP from 1982 to 2009 using both 8 km^2 AVHRR GIMMS from Tucker et al. (2005) and 1 km^2 MODIS net photosynthesis. A more recent version of GIMMS AVHRR NDVI (GIMMS 3g) data is available from 1981 to 2011 at 1/12th° spatial resolution.

10.3.4.2.1 Case Study

The strategy suggested by Steven et al. (2003) and Wessels (2009) was followed for calibrating 8 km^2 pixel resolution GIMMS annual ΣNDVI from 1982 to 2006 to MODIS NPP data aggregated from 1 to 8 km^2 using the 2000 to 2006 overlap period between these two

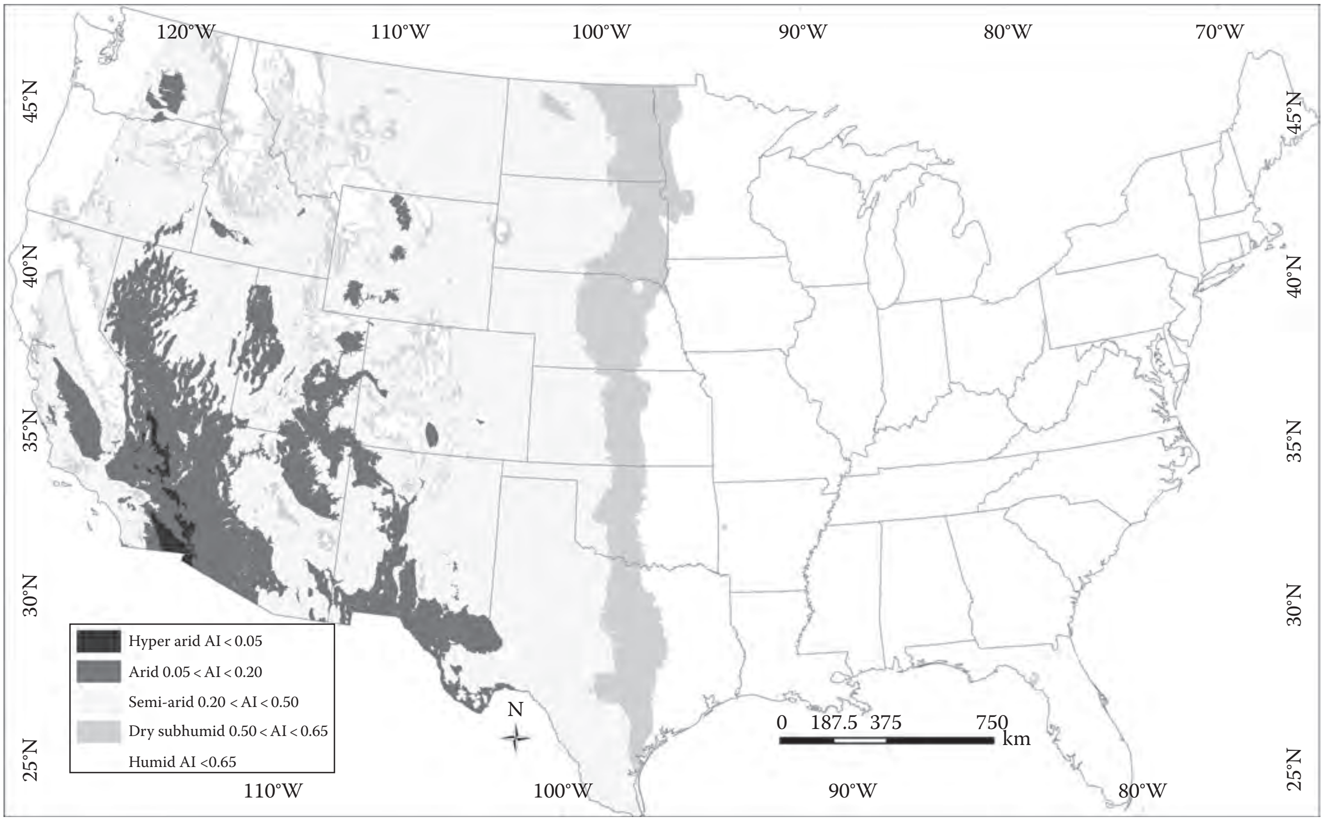

FIGURE 10.14 Distribution of aridity index (annual precipitation/potential evapotranspiration) classes throughout the United States used for aggregating NPP estimates for coterminous US rangelands.

time series. Collection 5 annual estimates of MODIS NPP from 2000 to 2006 and GIMMS ΣNDVI time series were subset to the rangeland portion of the contiguous United States and classified according to varying levels of aridity using AI (Figure 10.14). The AI of drylands (AI ≤ 0.65) is partitioned into four classes including the hyperarid, arid, semiarid, and dry subhumid classes.

10.3.4.2.1.1 Application and Validation of Linear Regression Approach The Taiga Earth Trend Modeler from IDRISI was used to conduct a simple linear regression on a pixel-by-pixel basis between the two time series using the years 2000, 2002, 2004, and 2006. This was done so that a holdout dataset could be retained for comparing predicted and observed NPP. Across all pixels in the rangeland domain, the mean NDVI was 0.03 and mean NPP was 281.6 g C m^{-2} $year^{-1}$. The mean equation across all pixels was

$$Y = 0.03 * X + (-31.7)$$

where

X is the annual GIMMS ΣNDVI

Y is the predicted 8 km^2 MODIS NPP and $r^2 = 0.41$ (Figure 10.15)

Panels A, B, and C in Figure 10.15 represent the estimated slope, intercept, and r^2 of a linear regression for each pixel in the study area between GIMMS NDVI and MODIS NPP for the years 2000, 2002, 2004, and 2006. Predicted MODIS NPP was subsequently compared to the observed MODIS NPP (Table 10.5). Figure 10.16 indicates a strong relationship between monthly integrated 8 km^2 GIMMS NDVI and monthly integrated 1 km^2 MODIS net photosynthesis (PSNnet) over the domain of coterminous US rangelands.

The net photosynthesis is a major component of the annual NPP product. To derive the final model to extend the NPP time series, the pixel-level regressions developed were applied to the annual GIMMS ΣNDVI from 1982 to 1999. To these data, the MODIS NPP time series from 2000 to 2009 were added, thus extending the final time series from 1982 to 2009.

Using the final time series, temporal and spatial variations in NPP response can be quantified. The mean NPP for each class from 1982 to 2009 was 95 ± 28 for hyperarid, 115 ± 47 for arid, 218 ± 114 for semiarid, and 370 ± 117 (g C m^{-2} $year^{-1}$) for the dry subhumid class. In addition, the temporal trend (not accounting for temporal autocorrelation) of NPP within each AI class was as follows: hyperarid ($r^2 = 0.08$, $p = 0.08$), arid ($r^2 = 0.01$, $p = 0.37$), semiarid ($r^2 = 0.25$, $p = 0.004$), and dry subhumid ($r^2 = 0.22$, $p = 0.006$) (Figure 10.17).

Using this approach, significant carbon gains were detected for both semiarid and arid systems. In addition, the positive response in arid and semiarid systems agrees with conclusions by Reeves and Baggett (2014) that significant increasing trends have been observed from 2000 to 2012 across much of the US rangeland domain, owed mostly to increased precipitation.

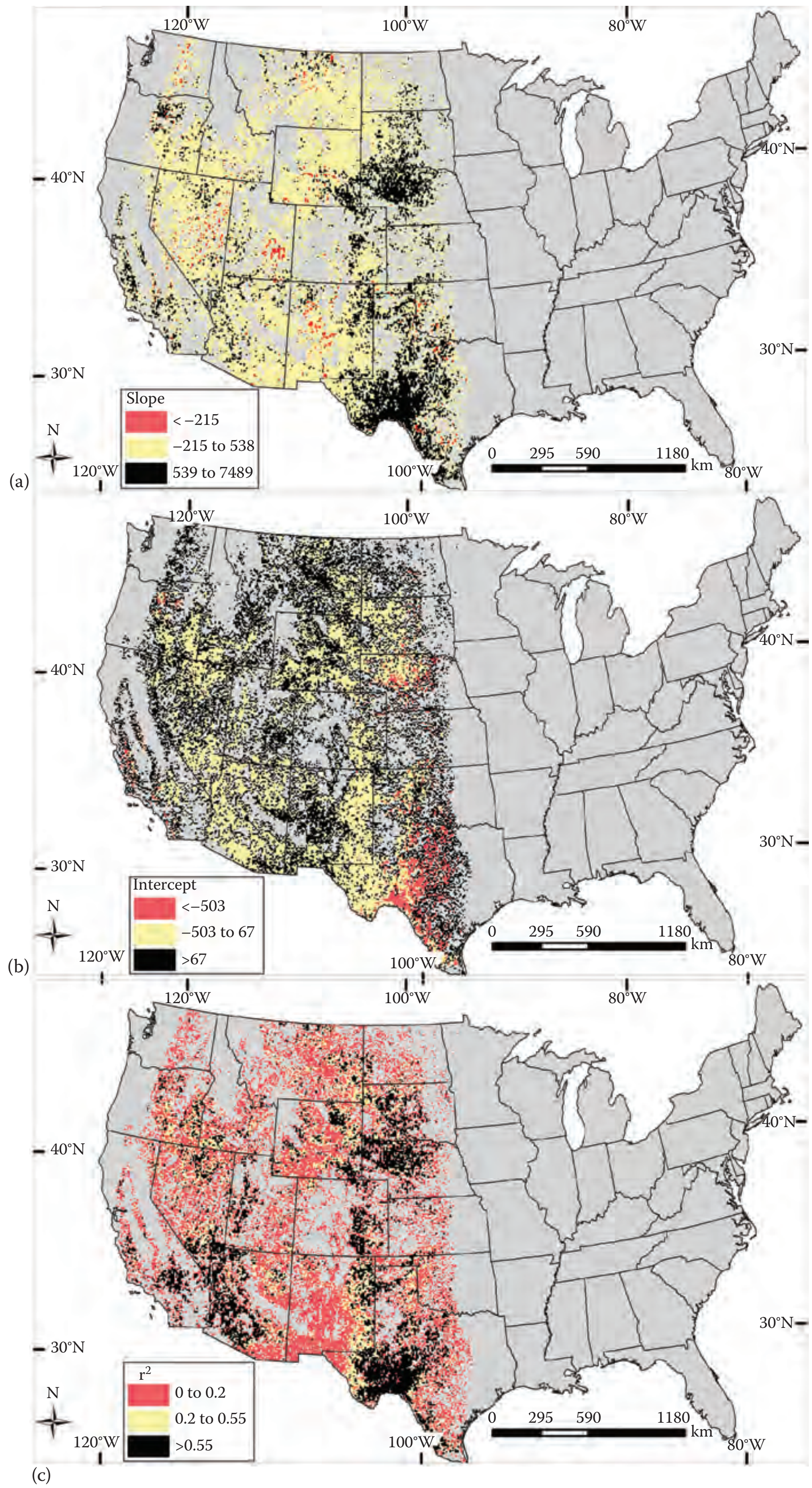

FIGURE 10.15 The resulting pixel-to-pixel linear regression models that were developed to calibrate GIMMS annual ΣNDVI to the MODIS NPP time series for the years 2000, 2002, 2004, and 2006. Panels (a), (b), and (c) represent the slope, intercept, and r^2 values for each pixel.

TABLE 10.5 Comparison of Predicted and Observed Values across the Extent of Rangelands in the Coterminous U.S. (g C m² year⁻¹)

	g C m² year⁻¹			
Year	Minimum	Median	Mean	SD
2001	16.5	179	211	123
	0.1	**186**	**220**	**137**
2003	15.3	189	218	131
	2.4	**184**	**217**	**131**
2005	19.8	236	126	126
	0.1	**210**	**157**	**157**

Bold numbers are predicted values based on the pixel level regression equations depicted in Figure 10.16.

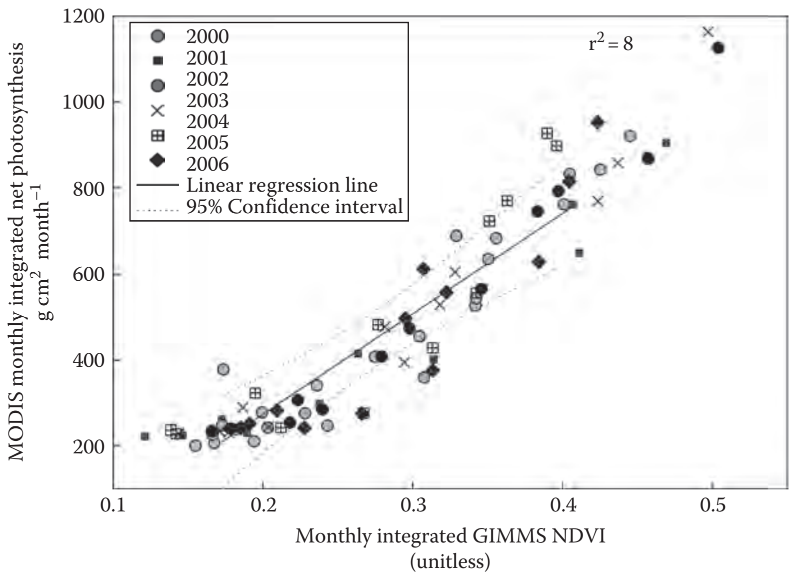

FIGURE 10.16 Relationship between monthly integrated MODIS-derived 1 km² net photosynthesis and GIMMS km² NDVI aggregated across all coterminous U.S. rangelands.

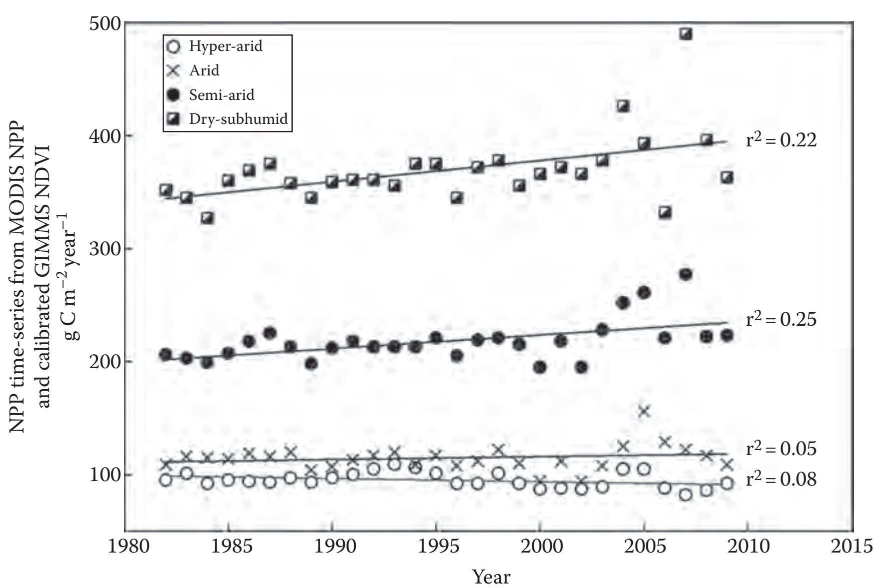

FIGURE 10.17 Rangeland mean NPP from 1982 to 2009 across four zones of AI including hyperarid, arid, semiarid, and dry subhumid.

The results portrayed in Figure 10.17 demonstrate improved chances for successfully interpreting vegetation response to global change through increasing the time series of satellite observation.

10.3.5 Remote Sensing of Global Land Cover

Global land cover data are essential to most global change research objectives, including the assessment of current global environmental conditions and the simulation of future environmental scenarios that ultimately lead to public policy development. In addition, land cover data are applied in national- and subcontinental-scale operational environmental and land management applications (e.g., weather forecasting, fire danger assessments, resource development planning, and the establishment of air quality standards). Land cover characteristics are integral to many Earth system processes (Hansen et al., 2000), in addition to providing information for carbon exchange and general circulation models. A common and important application of global land cover information is inference of biophysical parameters, such as LAI and fPAR, which influence global-scale climate and ecosystem process models. Use of these models and monitoring the state of the Earth's rangelands is needed for global change research, especially given the influence of growing anthropogenic disturbances (Lambin et al., 2001; Jung et al., 2006; Xie et al., 2008).

One of the remote-sensing community's grand challenges is to provide globally consistent but locally relevant land cover information (Estes et al., 1999). Evaluations of remote-sensing-based global land cover datasets have shown general agreement of patterns and total area of different land covers at the global level but have more limited agreement in spatial patterns at local to regional levels (McCullum et al., 2006) (Figure 10.18). Figure 10.18 demonstrates the difficulty in deriving rangeland

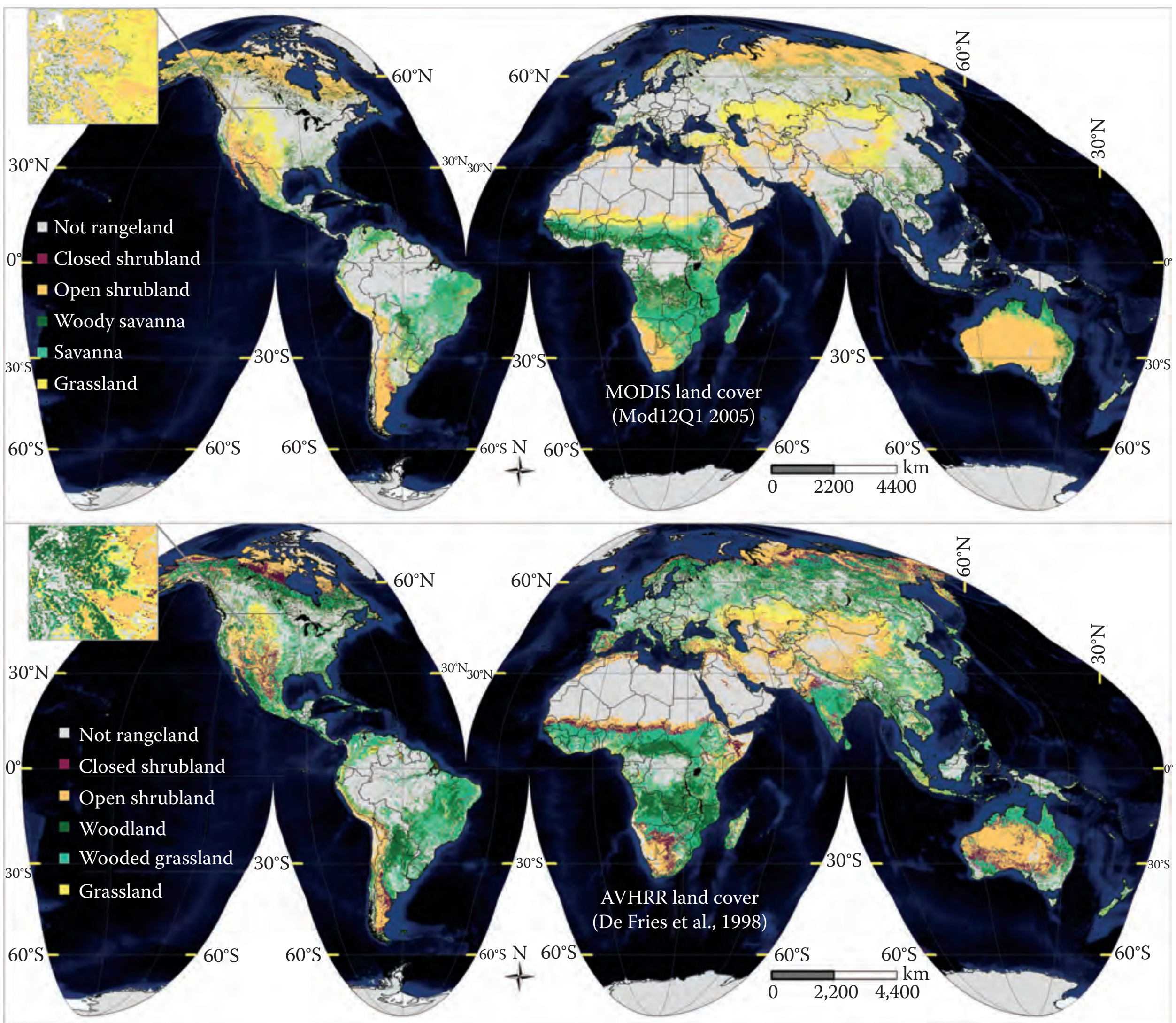

Figure 10.18 Comparison between 1 km² MODIS land cover data (Mod12Q1; UMD classification) and AVHRR-derived land cover (DeFries et al., 1998) using the simple biosphere model legend (Table 10.6).

area estimates using data from AVHRR (DeFries et al., 1998) and the MODIS Mod12Q1 (2005).

Both datasets have global coverage at 1 km^2 resolution but have different legends and classification techniques. Global mapping presents special challenges since the geographic variability of both land cover and remote-sensing inputs add complexity that can lead to inconsistent results. The evolution of global land cover datasets over the past 30 years has attempted to meet the grand challenge while adhering to general remote-sensing land cover–mapping standards dealing with accuracy, consistency, and repeatability.

The earliest contemporary efforts to provide global land cover data did not rely on remote-sensing inputs but instead was based on the developer's expertise and the quality of information from best available sources (Matthews, 1983; Olson, 1983; Wilson and Henderson-Sellers, 1985). These maps were coarse (i.e., $1° \times 1°$) in resolution but thematically detailed. Global land cover mapping based on remote sensing advanced rapidly in the 1990s when NOAA polar-orbiting data from the AHVRR were compiled into global coverage. Initially, 4 km^2 AVHRR Global Area Coverage Pathfinder data aggregated to $1° \times 1°$ (DeFries and Townshend, 1994) and later to 8 km^2 resolution (DeFries et al., 1998) were inputs to the first remote-sensing–based global land cover products.

The International Geosphere-Biosphere Programme (IGBP) served as the catalyst for a worldwide effort led by the USGS to generate a 1992–1993 set of 1 km^2 resolution AVHRR global 11-day maximum NDVI composites (Eidenshink and Faundeen, 1994). Also under IGBP auspices, these data were used to produce the first 1 km^2 resolution global land cover dataset using the 17-class International Geosphere-Biosphere Programme Global Land Cover Classification (IGBP DISCover) legend (Loveland et al., 2000) (Figure 10.18). Hansen et al. (2000) followed with the completion of a 1 km^2, 12-class land cover dataset (UMD land cover map). These two maps served as the foundation for future global-mapping initiatives since their development experiences and map strength and weaknesses provided valuable lessons for the next generation of maps.

The NASA Earth Observing System's ambitious global land product program based on multiresolution MODIS data established a new state of the art in global land cover mapping. MODIS global land cover based on 500 m resolution imagery and the 17-class IGBP DISCover legend started in the 2001 and since then has been updated annually (Friedl et al., 2002). This ongoing activity represents the only sustained global land cover initiative. In the 2000s, European global land cover projects contributed significantly to advancing global land cover understanding. The Global Land Cover 2000 (GLC2000) project used SPOT vegetation instrument data to produce a 22-class 1 km^2 resolution land cover dataset (Bartholomé and Belward, 2005). In a follow-on effort, the European Space Agency sponsored a follow-on project, GlobCover, that used ENVISAT MERIS imagery to generate the highest-resolution (300 m) global land dataset ever. The MERIS-based map contained 22 land cover classes based on the United Nations-sponsored international standard—land cover classification system (LCCS).

The most recent global land cover dataset is the unprecedented China-led Fine Resolution Observation and Monitoring of Global Land Cover (FROM-GLC) dataset that is based on Landsat 5 and 7 TM/ETM+ and other high-resolution Earth observation data spanning the first decade of the twenty-first century (Gong et al., 2013). The FROM-GLC dataset with 29 land cover classes establishes new standards for high-resolution land cover mapping and monitoring.

In addition to the thematic land cover mapping efforts described earlier (Table 10.6), global "continuous fields" products provide quantitative estimates of the percent tree cover within each grid cell. DeFries et al. (1999) developed global percent tree cover data using 1 km^2 AVHRR imagery, and Hansen et al. (2003) created similar products using MODIS.

10.3.5.1 Comparative Investigations of Global Land Cover Datasets

With a relatively large number of global land cover datasets available, users face a challenge in understanding which one is best suited for their application. The differences in spatial resolution, temporal properties, land cover legend, and quality complicate the selection. Land cover legend and quality are particularly significant factors. Accuracy assessments that provide insights into data quality are available for some of the global products. For example, both the IGBP DISCover and GLC2000 datasets were evaluated using an independent accuracy assessment. DISCover accuracy was measured at 66.9% (Scepan, 1999). Mayaux et al. (2006) determined that the overall GLC2000 product accuracy was 68.6%. The MODIS land cover dataset accuracy was assessed based on a comparison with training data, with the results showing 78.3% agreement (Friedl et al., 2002). The more recent GlobCover land cover dataset's (Table 10.6) independent accuracy was measured to be 73.0%. Finally, the China-led fine-resolution global land cover product was determined to have an overall accuracy of 71.5% (Gong et al., 2013). Accuracy assessments were not produced for UMD global land cover datasets.

The overall accuracies mask the significant variations in per class accuracies (e.g., Scepan, 1999 estimates that the DISCover individual class accuracies varied from 40% to 110%). The class accuracy variations, as well as variations in land cover legends and class definitions, make cover-specific applications problematic. As a response to this problem, a number of global dataset comparison studies have been undertaken, which focus on determining dataset strengths and weaknesses. Some have used independent datasets to look at regions or continents, such as Tchuenté et al.'s (2011) evaluation of GLC2000, GlobCover, and MODIS land cover for Africa and Frey and Smith's (2007) evaluation of IGBP DISCover and MODIS land cover over western Siberia. Other comparisons have looked at agreement between datasets across the globe. For example, Hansen and Reed (2000) compared UMD and IGBP DISCover products; Giri et al. (2005) compared MODIS and GLC2000; McCullum et al. (2006) compared IGBP, UMD, GLC2000, and MODIS products; and Fritz and See (2007) compared MODIS, GLC2000, and GlobCover.

TABLE 10.6 Summary of Characteristics of the Major Remote Sensing Global Land Cover Datasets

Database	Source	Vintage	Resolution	Land Cover Content (Suggested Rangeland Classes)	Strengths	Weaknesses
Global AVHRR NDVI land cover (De Fries and Townshend, 1994)	AVHRR	1987	1.0°[2] latitude	11 (3) land cover classes—based on simple biosphere model	First remote-sensing-based depiction of global land cover	Coarse resolution, applications limited to global circulation model applications.
Global AVHRR land cover (De Fries et al., 1998)	AVHRR Global Area Coverage Pathfi der	1987	8 km^2	14 (5) land cover classes—based on the simple biosphere model	Improved spatial resolution provided more realistic view of global land cover	Land cover classes were general and specific o one application requirement
IGBP DISCover (Loveland et al., 2000)	AVHRR local area coverage	1992–1993	1 km^2	17 (5) IGBP DISCover land cover classes and other land cover legends	Highest-resolution global land cover to date, validated based on statistical design	Variable image quality contributed to unevenness of land cover accuracy
UMD global land cover (Hansen et al., 2000)	AVHRR local area coverage	1992–1993	1 km^2	12 (5) land cover classes	Based on an automated analysis strategy	Not validated, affected by variable image quality
MODIS global land cover (Friedl et al., 2002)	MODIS	2001–present, produced annually	500 m^2	17 (5) IGBP DISCover land cover	Uses highest-quality remotely sensed inputs available, based on rigorous automated methods	Unknown accuracy due to the lack of a design-based map validation
GLC2000 (Bartholome and Belward, 2005)	SPOT 4 VEGETATION	2000	1 km^2	22 (5) land cover classes	Based on standardized land cover legend, validated results	Affected by variable image quality
GlobCover (Arino et al., 2007)	ENVISAT MERIS	2005–2006	300 m^2	22 (4) land cover classes, UN Land Cover Classifi ation System	Based on standardized land cover legend, validated results, and highest-resolution imagery to date	Regional variability in image quality increased uncertainty of results in some parts of the world
Fine resolution global land cover (Gong et al., 2013)	Landsat 5 and 7	Nominally 2005–2006	30 m^2	29 (6) land cover classes	Highest-resolution dataset ever produced	Limited temporal inputs resulted in regional inconsistencies

McCullum et al. (2006) concluded that while there is general agreement at the global level in total area and general land cover patterns; there is limited agreement when looking at specific spatial distributions.

Perhaps the most definitive effort to understand the difference in global datasets comes from Herold et al. (2008). In this study, the IGBP DISCover, UMD, GLC2000, and MODIS land cover datasets were harmonized by crosswalking the different land cover classes to a common classification standard—the UN LCCS (Di Gregorio, 2005). Thirteen classes were defined, and the original accuracy assessment samples associated with the various products were used to determine per class and overall accuracy for each harmonized product. Cover types with large homogeneous extents, such as barren, cultivated, and managed, shrublands, and snow and ice, are more consistently represented in global products than smaller, discontinuous classes. All products show a limited ability to consistently represent mixed classes.

As the quality and resolution of remotely sensed data used for global land cover mapping improves, the logical expectation is that overall and individual class accuracies will also improve. Fritz et al. (2011) emphasize the continued uncertainty in global land cover products, especially in land cover classes associated with agriculture and some forest groups. They suggest that increased use of in situ data is the key to improving global land cover datasets.

10.4 Future Pathways of Global Sensing in Rangeland Environments

Remote sensing has created unprecedented capacity to study the Earth by providing repeated measurements of biological phenomena at global scales. Since the first regional applications of NDVI (one of the earliest regional applications found is Rouse et al., 1973) (Section 10.2), the study of the global rangeland situation has benefitted greatly from advancements made in a relatively short period of time. Though future uses of remote-sensing data will be used in unexpected ways, obvious areas of enhancement and progress are anticipated. These future pathways can be expressed in distinct areas including data availability, processing improvement, and biophysical product improvement.

The design and intended application of spaceborne sensors will continue to evolve, and a wider variety of satellite systems including radar and lidar could be quite beneficial in the future. If the past provides a glimpse into the future, new sensors with improved capabilities will be developed, but it is unclear, however, whether improved spatial, spectral, and temporal resolution of satellite remote sensing will provide the greatest advancements in the evaluations of rangelands on a global scale. The ability to extract surface features and quantify biophysical properties will still be limited by the same factors presently hindering remote sensing of rangelands. Characteristics such as soil background, leaf anatomy and physiology, and relatively low biomass conspire to hinder remote sensing of rangelands. Very little can be done to change these situations, and as a result, future pathways should include a focus on data continuity, increased data availability, better computer processing systems, and global campaigns for collecting field-referenced data.

Remote-sensing data continuity is important to monitoring global rangelands, and loss of this critical aspect will significantly weaken our ability to understand what the biosphere is indicating. The need for continuity is recognized in the Land Remote Sensing Policy Act of 1992, which states

> The continuous collection and utilization of land remote sensing data from space are of major benefit in studying and understanding human impacts on the global environment, in managing the Earth's resources, in carrying out national security functions, and in planning and conducting many other activities of scientific, economic, and social importance.

Since the first civilian spaceborne missions (e.g., Landsat 1), the global monitoring community and government agencies have been reasonably successful in providing the needed continuity. The Landsat program is a good example of the flow and continuity with incremental improvements with each successive launch generally maintaining a 30 m^2 resolution benchmark. If archive data from Landsat 4 (deployed in 1982) are included, 32 years of 30 m^2 spatial resolution from the TM sensor in visible and NIR (at the minimum) are available. Landsat 8, launched on February 11, 2013, is the most recent addition to the suite of Landsat satellite launches and provides an example of maintaining continuity with previous missions while improving capability. Landsat 8 contains the Operational Land Imager (OLI) and the Thermal Infrared Sensor (TIRS), which provide global coverage at varying resolutions. The OLI provides two new spectral bands for detecting cirrus clouds and the other for coastal zone observations. Now that the entire archive of Landsat data has been made freely and publically available, usage has increased exponentially. The unprecedented data availability has and will continue to lead to new algorithmic and ecological discoveries.

Increased data usage may signal greater interest in remote sensing but certainly tracks the increased microprocessor speed over the last decade (Figure 10.19). As processing speed and memory have increased so has the level of algorithmic sophistication and spatial domain for analysis. Indeed, the global remote-sensing community is poised for improved characterization capabilities, due to new data policies and concurrent advances in computing (Hansen and Loveland, 2011).

Even a decade ago, it would have been unthinkable to regularly process and store a global time series of satellite imagery with a pixel resolution of less than about 250 m^2. Although it is certainly possible to monitor rangelands globally at 30 m^2, it will be a monumental task. Each TM path/row contains 0.534 GB in the seven multispectral and thermal channels and approximately 0.234 GB for the panchromatic band. Since roughly 16,396

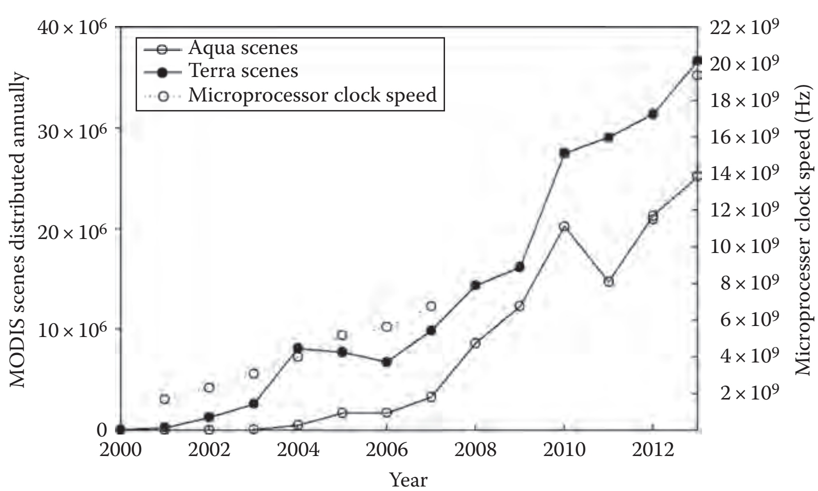

FIGURE 10.19 Microprocessor speed and MODIS data usage (microprocessor speed data courtesy of https://www.raptureready.com/accessed April 1, 2014; MODIS usage data courtesy of B. Ramachandran NASA Earth Observing System, LP DAAC.)

TABLe 10.7 Spectral Channels and Suggested Usefulness

					Horiz. Sample Interval (km) (Track × Scan)	
		Band No.	Driving EDR(s)	Spectral Range (μm)	Nadir	End of Scan
Refl ctive bands	VisNIR	M1	Ocean color aerosol	0.402–0.422	0.742 × 0.259	1.60 × 1.58
		M2	Ocean color aerosol	0.436–0.454	0.742 × 0.259	1.60 × 1.58
		M3	Ocean color aerosol	0.478–0.498	0.742 × 0.259	1.60 × 1.58
		M4	Ocean color aerosol	0.545–0.565	0.742 × 0.259	1.60 × 1.58
		I1	Imagery EDR	0.600–0.680	0.371 × 0.387	0.80 × 0.789
		M5	Ocean color aerosol	0.662–0.682	0.742 × 0.259	1.60 × 1.58
		M6	Atmospheric correction	0.739–0.754	0.742 × 0.776	1.60 × 1.58
		I2	NDVI	0.846–0.885	0.371 × 0.387	0.80 × 0.789
		M7	Ocean color aerosol	0.846–0.885	0.742 × 0.259	1.60 × 1.58
	S/WMIR	M8	Cloud particle size	1.230–1.250	0.742 × 0.776	1.60 × 1.58
		M9	Cirrus/cloud cover	1.371–1.386	0.742 × 0.776	1.60 × 1.58
		I3	Binary snow map	1.580–1.640	0.371 × 0.387	0.80 × 0.789
		M10	Snow fraction	1.580–1.640	0.742 × 0.776	1.60 × 1.58
		M11	Clouds	2.225–2.275	0.742 × 0.776	1.60 × 1.58
Emissive Bands		I4	Imagery clouds	3.550–3.930	0.371 × 0.387	0.80 × 0.789
		M12	SST	3.660–3.840	0.742 × 0.776	1.60 × 1.58
		M13	SST fi es	3.973–4.128	0.742 × 0.259	1.60 × 1.58
	LWIR	M14	Cloud top properties	8.400–8.700	0.742 × 0.776	1.60 × 1.58
		M15	SST	10.263–11.263	0.742 × 0.776	1.60 × 1.58
		I5	Cloud imagery	10.500–12.400	0.371 × 0.387	0.80 × 0.789
		M16	SST	11.538–12.488	0.742 × 0.776	1.60 × 1.58

The LWIR are long-wave infrared bands while the S/MWIR are short- to mid-wave infrared bands.
Source: Adapted from Schueler et al. (2003).

scenes are required for global coverage (including oceans), that is an estimated 12.3 TB of data for a single 16-day period. The repeat frequency or revisit cycle is 16 days (~22 periods per year), so the total amount of data since 1999 is near 4208 TB. Based on an online storage price of $0.08 per month per GB (https://cloud.google.com/products/cloud-storage/), the storage cost is tantamount to roughly 4 million dollars per year. While this represents a significant amount of data and resources, a growing number of global applications at 30 m^2 spatial resolution can be expected. Indeed, this past year has seen the production of a Landsat-based global database of tree cover at 30 m^2 resolution (Sexton et al., 2013), and work is underway to develop long-term (Landsat period of record) land cover dynamics on a global scale (Sexton et al., 2013).

Presently, numerous efforts aimed at global remote sensing of rangelands are based on MODIS sensors aboard the Terra and Aqua satellites. Since 2006, the number of scenes annually distributed from MODIS data from both Aqua and Terra has increased by 7.6 million per year (about 181 TB year^{-1}) (Figure 10.19). This use is a testament to the breadth of vetted science data products offered globally. Continuity between MODIS and future global Earth-observing satellites is provided by the Suomi National Polar-orbiting Partnership (NPoP) satellite. Suomi NPoP was launched in 2011 with five key instruments, but the instrument with greatest application, to rangelands globally, and similarity with the AVHRR and MODIS predecessors is the VIIRS. The VIIRS instrument observes the Earth and atmosphere at 22 visible and infrared wavelengths (Table 10.7). Suomi NPP is the bridge between the current NASA research Earth-observing satellites and future NOAA missions, specifically the Joint Polar Satellite System (JPSS) (Lee et al., 2006). The JPSS is a joint program between NOAA, NASA, and the Defense Weather Satellite System, tasked with developing the next-generation requirements for environmental research, weather forecasting, and climate monitoring (npp.gsfc.nasa.gov/viirs.html). The JPSS provides operational continuity of satellite-based observations and products through a series of advanced spacecraft of which Suomi NPoP is a member. The next two satellites to be launched include JPSS 1 and JPSS 2, both of which will contain, among others, the VIIRS instrument. The JPSS 1 platform is scheduled to be launched in 2017, while JPSS 2 is scheduled for launch in 2021.

The continuity of land remote-sensing instruments is well established and provides a critical component to researchers involved with global change research in rangeland environments. Most future global issues will emulate present concerns. In other words, the problems, or area of focus, today (e.g., vegetation trends, land degradation, and fire processes) will continue and perhaps intensify in the future.

Regardless of the increasingly important roles remote sensing will play, georeferenced field data will play an equally critical aspect of biospheric monitoring (Baccini et al., 2007). Fritz and See (2011) suggest that increased use of in situ data is the key to improving global datasets. The collection, maintenance, analysis, and distribution of georeferenced field data, however, are a time-consuming and resource-intensive exercise, especially over regional or global domains. In this vein, the citizen scientist is an underutilized concept that can be cheaply and effectively employed to globally collect biospheric observations. Citizen science can be defined as

> the systematic collection and analysis of data; development of technology; testing of natural phenomena; and the dissemination of these activities by researchers on a primarily avocational basis.
>
> **OpenScience (2011)**

These open networks promote interactions between scientists, society, and policymakers leading to decision making by scientific research conducted by amateur or nonprofessional scientists (Socientize, 2013). Advancements in communication and technology are credited with aiding the growth of citizen scientists (Silverton, 2009). Collectively, citizen science efforts from around the globe could possibly provide powerful venues for validating and calibrating future remote-sensing efforts.

10.5 Conclusions

Rangelands are found extensively throughout the world covering about 50% of the global land mass. The remoteness, harsh conditions, and high interannual variation in productivity make remote sensing the most cost-effective and efficacious tool for evaluating the status and health of rangelands globally. Global remote sensing has unique constraints from a remote-sensing perspective and spatial resolution is often sacrificed in place of temporal resolution. A broad suite of sensors possessing various spectral channels, revisit times, and spatial resolutions are available for regional to global rangeland applications. However, most global applications, especially those sponsored for national or international applications (e.g., LADA, IGBP), use AVHRR, SPOT-VGT, MODIS, and to a lesser degree TM. Additionally, a large number of biophysical phenomena can be investigated with the myriad of sensors, but as discussed in this chapter, we focused on the globally relevant issues of degradation, fire, land cover, food security, and global change. In this chapter, we demonstrate sensors, data, algorithms, strengths, and limitations of various methods to address these globally significant issues.

Though estimates vary, the proportion of degraded rangelands is around 23% globally (Table 10.4). The use and interpretation of RUE for evaluating degradation patterns is controversial (Prince et al., 2007), but alternative techniques are subject to similar issues and assumptions. Thus, when considering degradation, especially in a global context, a model ensemble approach (e.g., combine local NPP scaling, rainfall use efficiency, and NPP trend analysis) may be most useful to indicate trends and identify where action is needed to lessen detrimental effects on goods and services.

Most global land cover efforts have limited thematic resolution of rangeland classes (average number of rangeland classes is 4.75; Table 10.6). However, computational resources and algorithmic complexity is sufficient to produce higher spatial and thematic resolution land cover maps as inaugurated by studies such as Gong et al. (2013) and Hansen et al. (2013). Land cover and land use will continue to evolve in response to broadscale disturbance and global change. As a result, monitoring global change and extent and severity of fire has been the focus of many algorithms, national programs, and sensors. As an example, the MODIS sensor aboard both the Terra and Aqua platforms was designed with fire monitoring in mind with channels 21, 22, 31, and 33. Burn severity evaluation is a relatively new capability since the AVHRR and SPOT-VGT sensors lack the spectral channels necessary for contemporary algorithms. Likewise, the advent of the MODIS—derived NPP product (Running et al., 2004)—has spawned numerous studies aimed at evaluating NPP patterns globally. In this chapter, we demonstrate rather unchanged NPP trajectories in the rangeland domain but also identify cases where higher spatial and thematic resolution products are needed to further understand patterns. Despite these relatively unchanged temporal trajectories globally, drought and degradation are detrimental on a regional basis and regularly threaten the security of food derived from rangelands. The LEWS, driven by MODIS-derived 250 m^2 NDVI, is a useful program to provide guidance local governments and international aid organizations. As world population continues to grow, it is likely that the programs like LEWS will become increasingly important. These issues emphasize the critical importance of mission and spectral continuity. The recent launch of Landsat 8 and Suomi NPoP is a critical stepping stone to future efforts, but compared to their predecessors, they possess a distinctive lack of present use, given their recent recentness.

References

Al-Bakri, J. T. and J. C. Taylor. 2003. Application of NOAA AVHRR for monitoring vegetation conditions and biomass in Jordan. *Journal of Arid Environments*, 54, 579–593.

Allbed, A. and L. Kumar. 2013. Soil salinity mapping and monitoring in arid and semi-arid regions using remote sensing technology: A review. *Advances in Remote Sensing*, 2, 373–385.

Allen, J. L. and B. Sorbel. (2008). Assessing the differenced Normalized Burn Ratio's ability to map burn severity in the boreal forest and tundra ecosystems of Alaska's national parks. *International Journal of Wildland Fire*, 17, 463–475.

An, N., K. P. Price, and J. M. Blair. (2013). Estimating aboveground net primary productivity of the tallgrass prairie ecosystem of the Central Great Plains using AVHRR NDVI. *International Journal of Remote Sensing*, 34, 3717–3735.

Angerer, J. P. (2008). Examination of high resolution rainfall products and satellite greenness indices for estimating patch and landscape forage biomass. *PhD Dissertation*. Texas A&M University, College Station, Texas.

Angerer, J. 2012. Gobi forage livestock early warning system. In *Conducting National Feed Assessments*, eds. M. B. Coughenour and H. P. S. Makkar, pp. 115–130. Rome, Italy: Food and Agriculture Organization.

Arino, O., D. Gross, F. Ranera, L. Bourg, M. Leroy, P. Bicheron, and R. Witt. (2007). *GlobCover: ESA service for global land cover from MERIS.* International Geoscience and Remote Sensing Symposium, Barcelona, Spain. pp. 2412–2415.

Arino, O., S. Casadio, and D. Serpe. 2012. Global night-time fire season timing and fire count trends using the ATSR instrument series. *Remote Sensing of Environment*, 116, 226–238.

Awuma, K. S., J. W. Stuth, R. Kaitho, and J. Angerer. (2007). Application of Normalized Differential Vegetation Index and geostatistical techniques in cattle diet quality mapping in Ghana. *Outlook on Agriculture*, 36, 205–213.

Baccini, A., M. A. Friedl, C. E. Woodcock, and Z. Zhu. 2007. Scaling fi ld data to calibrate and validate moderate spatial resolution remote sensing models. *Photogrammetric Engineering and Remote Sensing*, 73, 945–954.

Bai, E., T. W. Boutton, X. B. Wu, F. Liu, and S. R. Archer. 2009. Landscape-scale vegetation dynamics inferred from spatial patterns of soil δ13C in a subtropical savanna parkland. *Journal of Geophysical Research*, 114, G01019.

Bai, Z. G., D. L. Dent, L. Olsson, and M. E. Schaepman. 2008. Proxy global assessment of land degradation. *Soil Use and Management*, 24, 223–234.

Barbosa, P. M., J. M. Grégoire, and J. M. C. Pereira. 1999. An algorithm for extracting burned areas from time series of AVHRR GAC data applied at a continental scale. *Remote Sensing of Environment*, 69, 253–263.

Bartholomé, E. and A. S. Belward. 2005. GLC2000: A new approach to global land cover mapping from Earth observation data. *International Journal of Remote Sensing*, 26, 1959–1977.

Bauer, M. E. 1976. Technological basis and applications of remote sensing of the Earth's resources. *IEEE Transactions on Geoscience Electronics*, 14, 3–9.

Beatriz, A. and F. Valladares. 2008. International efforts on global change research. In *Earth Observation of Global Change: The Role of Satellite Remote Sensing in Monitoring the Global Environment*, ed. E. Chuvieco, pp. 1–21. Dordrecht, the Netherlands: Springer.

Blanco, P., H. d. Valle, P. Bouza, G. Metternicht, and L. Hardtke. 2014. Ecological site classifi ation of semiarid rangelands: Synergistic use of Landsat and Hyperion imagery. *International Journal of Applied Earth Observation and Geoinformation*, 29, 11–21.

Carreiras, A., M. Vasconcelos, and R. Lucas. 2012. Understanding the relationship between aboveground biomass and ALOS PALSAR data in the forests of Guinea-Bissau (West Africa). *Remote Sensing of Environment*, 121, 426–442.

Carter, L. J. 1969. Earth resources satellite: Finally off the ground? *Science*, 163, 796–798.

Chuvieco, E. and R. G. Congalton. 1988. Mapping and inventory of forest fi es from digital processing of TM data. *Geocarto International*, 3, 41–53.

Chuvieco, E., D. Riano, I. Aguado, and D. Cocero. (2002). Estimation of fuel moisture content from multitemporal analysis of Landsat Thematic Mapper refl ctance data: applications in fi e danger assessment. *International Journal of Remote Sensing*, 23, 2145–2162.

Crist, E. P. and R. C. Cicone. 1984. Application of the tasseled cap concept to simulated Thematic Mapper data. *Photogrammetric Engineering and Remote Sensing*, 50, 343–352.

Deering, D. W., J. W. Rouse, R. H. Haas, and J. A. Schell. 1975. Measuring forage production of grazing units from Landsat MSS data. In *Tenth International Symposium on Remote Sensing of Environment*, pp. 1169–1178. Ann Arbor, MI: University of Michigan.

DeFries, R. S., M. Hansen, J. R. G. Townshend, and R. Solberg. 1998. Global land cover classifi ations at 8 km spatial resolution: The use of training data derived from Landsat imagery in decision tree classifie s. *International Journal of Remote Sensing*, 19, 3141–3168.

DeFries, R. S. and J. R. G. Townshend. 1994. NDVI-derived land cover classifi ations at a global scale. *International Journal of Remote Sensing*, 15, 3567–3586.

DeFries, R. S., J. R. G. Townshend, and M. C. Hansen. 1999. Continuous fi lds of vegetation characteristics at the global scale at 1-km resolution. *Journal of Geophysical Research: Atmospheres*, 104, 16911–16923.

Di Gregorio, A. 2005. *Land Cover Classification System: Classification Concepts and User Manual: LCCS*. Rome, Italy: Food & Agriculture Organization.

Dong, J., X. Xiao, S. Sheldon, C. Biradar, G. Zhang, N. D. Duong, M. Hazarika, K. Wikantika et al. 2014. A 50-m forest cover map in southeast Asia from ALOS/PALSAR and its application on forest fragmentation assessment. *PLoS ONE*, 9, e8580. doi:10.1371/journal.pone.0085801.

Dungan, J. 1998. Spatial prediction of vegetation quantities using ground and image data. *Remote Sensing*, 19, 267–285.

Dwyer, E., S. Pinnock, J. M. Gregorie, and J. M. C. Pereira. 2000. Global spatial and temporal distribution of vegetation fi e as determined from satellite observations. *International Journal of Remote Sensing*, 21, 1289–1302.

Eidenshink, J., B. Schwind, K. Brewer, Z. Zhu, B. Quayle, and S. Howard. 2007. A project for monitoring trends in burn severity. *Fire Ecology*, 3, 3–19.

Eidenshink, J. C. and J. L. Faundeen. 1994. The 1 km AVHRR global land data set: First stages in implementation. *International Journal of Remote Sensing*, 104, 3443–3462.

Elvidge, C. D. and R. J. P. Lyon. 1985. Influence of rock soil spectral variation on the assessment of green biomass. *Remote Sensing of Environment*, 17, 265–279.

Estes, J., A. Belward, T. Loveland, J. Scepan, A. Strahler, J. Townshend, and C. Justice. 1999. The way forward. *Photogrammetric Engineering and Remote Sensing*, 65, 1089–1093.

Everitt, J. H., C. Yang, R. Fletcher, and C. J. Deloach. 2008. Comparison of QuickBird and SPOT 5 satellite imagery for mapping giant reed. *Journal of Aquatic Plant Management*, 46, 77–82.

Fang, H. and W. Ping. 2010. Vegetation change of ecotone in west of northeast china plain using time-series remote sensing data. *Chinese Geographical Society*, 20, 167–175.

Fava, F., R. Colombo, S. Bocchi, and C. Zucca. 2012. Assessment of Mediterranean pasture condition using MODIS normalized difference vegetation index time series. *Journal of Applied Remote Sensing*, 6, 063530-1-063530-12.

Fensholt, R., K. Rasmussen, T. T. Nielsen, and C. Mbow. (2009). Evaluation of earth observation based long term vegetation trends—Intercomparing NDVI time series trend analysis consistency of Sahel from AVHRR GIMMS, Terra MODIS and SPOT VGT data. *Remote Sensing of Environment*, 113, 1886–1898.

Fensholt, R. and S. R. Proud. 2012. Evaluation of Earth observation based global long term vegetation trends—Comparing GIMMS and MODIS global NDVI time series. *Remote Sensing of Environment*, 119, 131–147.

Fensholt, R. and K. Rasmussen. 2011. Analysis of trends in the Sahelian 'rain-use efficiency' using GIMMS NDVI, RFE and GPCP rainfall data. *Remote Sensing of Environment*, 115, 438–451.

Fensholt, R. I., M. S. Sandholt, S. Rasmussen, S. Stisen, and A. Diou. 2006. Evaluation of satellite based primary production modeling in the semi-arid Sahel. *Remote Sensing of Environment*, 105, 173–188.

Flasse, S. and P. Ceccato. 1996. A contextual algorithm for AVHRR fi e detection. *International Journal of Remote Sensing*, 17, 419–424.

Foley, J., R. DeFries, and G. P. Asner. 2005. Global consequences of land use. *Science*, 309, 570–574.

Foody, G. M. 2003. Geographical weighting as a further refi ement to regression modelling: An example focused on the NDVI–rainfall relationship. *Remote Sensing of Environment*, 88, 283–293.

Fox, W. E., D. W. McCollum, J. E. Mitchell, L. E. Swanson, U. P. Kreuter, J. A. Tanaka, G. R. Evans, and H. T. Heintz. (2009). An Integrated Social, Economic, and Ecologic Conceptual (ISEEC) Framework for Considering Rangeland Sustainability. *Society & Natural Resources*, 22, 593–606.

Frank, T. D. 1984. Assessing change in the surficial character of a semiarid environment with Landsat residual images. *Photogrammetric Engineering and Remote Sensing*, 50, 471–480.

French, N. H. F., J. L. Allen, R. J. Hall, E. E. Hoy, E. S. Kasischke, K. A. Murphy, and D. L. Verbyla. 2008. Using Landsat data to assess fi e and burn severity in the North American boreal forest region: An overview. *International Journal of Wildland Fire*, 17, 443–462.

Frey, K. E. and L. C. Smith. 2007. How well do we know northern land cover? Comparison of four global vegetation and wetland products with a new ground-truth database for West Siberia. *Global Biogeochemical Cycles*, 21, 1–15.

Friedl, M. A., D. K. McIver, J. C. F. Hodges, X. Y. Zhang, D. Muchoney, A. H. Strahler, C. E. Woodcock, S. Gopal et al. 2002. Global land cover mapping from MODIS: Algorithms and early results. *Remote Sensing of Environment*, 83, 287–302.

Friedl, M. A., D. Sulla-Menashe, B. Tan, A. Schneider, N. Ramankutty, A. Sibley, and X. M. Huang. (2010). MODIS Collection 5 global land cover: Algorithm refi ements and characterization of new datasets. *Remote Sensing of Environment*, 114, 168–182.

Fritz, S. and L. M. See. 2007. Identifying and quantifying uncertainty and spatial disagreement in the comparison of Global Land Cover for different applications. *Global Change Biology*, 14, 1057–1075.

Fritz, S., L. See, I. McCallum, C. Schill, M. Obersteiner, M. van der Velde, H. Boettcher, P. Havlík et al. 2011. Highlighting continued uncertainty in global land cover maps for the user community. *Environmental Research Letters*, 6, 1–7.

Fry, J., G. Xian, S. Jin, J. Dewitz, C. Homer, L. Yang, C. Barnes, N. Herold et al. 2011. Completion of the 2006 national land cover database for the conterminous United States. *Photogrammetric Engineering and Remote Sensing*, 77, 858–864.

Gallo, K., L. Li, B. Reed, J. Eidenshink, and J. Dwyer. (2005). Multi-platform comparisons of MODIS and AVHRR normalized difference vegetation index data. *Remote Sensing of Environment*, 99, 221–231.

Ganguly, S., A. Samanta, M. A. Schull, N. V. Shabanov, C. Milesi, R. R. Nemani, Y. Knyazikhin, and R. B. Myneni. 2008. Generating vegetation leaf area index Earth system data record from multiple sensors. Part 2: Implementation, analysis and validation. *Remote Sensing of Environment*, 112, 4318–4332.

Geerken, R., N. Batikha, D. Celisj, and E. Depauw. 2005. Differentiation of rangeland vegetation and assessment of its status: Field investigations and MODIS and SPOT VEGETATION data analyses. *International Journal of Remote Sensing*, 26, 4499–4526.

Giglio, L., J. Descloitres, C. O. Justice, and Y. J. Kaufman. 2003. An enhanced contextual fi e detection algorithm for MODIS. *Remote Sensing of Environment*, 87, 272–282.

Giglio, L., T. Loboda, D. P. Roy, B. Quayle, and C. O. Justice. 2009. An active-fi e based burned area mapping algorithm for the MODIS sensor. *Remote Sensing of Environment*, 113, 408–420.

Gilbert, N. 2011. Science enters desert debate. *Nature*, 447, 262.

Giri, G., Z. L. Zhu, and B. Reed. 2005. A comparative analysis of the global land cover 2000 and MODIS land cover data sets. *Remote Sensing of Environment*, 94, 123–132.

Gong, P., J. Wang, L. Yu, Y. Zhao, Y. Zhao, L. Liang, Z. Niu, X. Huang et al. 2013. Finer resolution observation and monitoring of global land cover: First mapping results with Landsat TM and ETM+ data. *International Journal of Remote Sensing*, 34, 2607–2654.

Graetz, R. D. 1987. Satellite remote-sensing of Australian rangelands. *Remote Sensing of Environment*, 23, 313–331.

Graetz, R. D., D. M. Carneggie, R. Hacker, C. Lendon, and D. G. Wilcox. 1976. A qualitative evaluation of LANDSAT imagery of Australia rangelands. *Australian Rangeland Journal*, 1, 53–59.

Graetz, R. D., M. R. Gentle, R. P. Pech, J. F. O'Callaghan, and G. Drewien. 1983. The application of Landsat image data to rangeland assessment and monitoring: An example from South Australia. *Australian Rangeland Journal*, 5, 63–73.

Graetz, R. D., R. P. Pech, and A. W. Davis. 1988. The assessment and monitoring of sparsely vegetated rangelands using calibrated Landsat data. *International Journal of Remote Sensing*, 9, 1201–1222.

Graetz, R. D., R. P. Pech, M. R. Gentle, and J. F. Ocallaghan. 1986. The application of Landsat image data to rangeland assessment and monitoring—The development and demonstration of a land image-based resource information-system (LIBRIS). *Journal of Arid Environments*, 10, 53–80.

Gray, T. I. and D. G. McCrary, 1981. The environmental vegetation index, a tool potentially useful for arid land management. *AgRISTAR Report No. EW-N-1-04076*, Johnson Space Center, Houston, Texas 17132. 7 pp.

Hacker, R. 1980. Prospects for satellite applications in Australian rangelands. *Tropical Grasslands*, 14, 289.

Hansen, M. C., R. S. DeFries, J. R. G. Townshend, M. Carroll, C. Dimiceli, and R. A. Dimiceli. 2003. Global percent tree cover at a spatial resolution of 500 meters: First results of the MODIS vegetation continuous fi lds algorithm. *Earth Interactions*, 7, 1–15.

Hansen, M. C., R. S. DeFries, J. R. G. Townshend, and R. Sohlberg. 2000. Global land cover classifi ation at the 1 km spatial resolution using a classifi ation tree approach. *International Journal of Remote Sensing*, 21, 1331–1364.

Hansen, M. C. and T. R. Loveland. 2011. A review of large area monitoring of land cover change using Landsat data. *Remote Sensing of Environment*, 122, 66–74.

Hansen, M. C., P. V. Potapov, R. Moore, M. Hancher, S. A. Turubanova, A. Tyukavina, D. Thau, S. V. Stehman et al. 2013. High-Resolution global maps of 21st-century forest cover change. *Science*, 342, 850–853.

Hansen, M., and B. Reed, (2000). A comparison of the IGBP DISCover and University of Maryland 1 km global land cover products. *International Journal of Remote Sensing*, 21, 1365–1373.

Herold, M., P. Mayaux, C. E. Woodcock, A. Baccini, and C. Schmullius. 2008. Some challenges in global land cover mapping: An assessment of agreement and accuracy in existing 1 km datasets. *Remote Sensing of the Environment*, 112, 2538–2556.

Holmgren, M., and M. Scheffer. (2001). El Niño as a Window of Opportunity for the Restoration of Degraded Arid Ecosystems. *Ecosystems*, 4, 151–159.

Holmgren, M., P. Stapp, C.R. Dickman, C. Gracia, S. Graham, J. R. Gutiérrez, C. Hice, F. Jaksic, D. A. Kelt, M. Letnic, M. Lima, B. C. López, P. L. Meserve, W. B. Milstead, G. A. Polis, M. A. Previtali, M. Richter, S. Sabaté, and F. A. Squeo, (2006). Extreme climatic events shape arid and semiarid ecosystems. *Frontiers in Ecology and the Environment*, 4, 87–95.

Homer, C. G., R. D. Ramsey, T. C. Edwards, and A. Falconer. 1997. Landscape cover-type modeling using a multi-scene thematic mapper mosaic. *Photogrammetric Engineering and Remote Sensing*, 63, 59–67.

Huete, A. R. 1988. A soil-adjusted vegetation index (SAVI). *Remote Sensing of Environment*, 25, 295–309.

Huete, A., K. Didan, T. Miura, E. P. Rodriguez, X. Gao, and L. G. Ferreira. 2002. Overview of the radiometric and biophysical performance of the MODIS vegetation indices. *Remote Sensing of Environment*, 83, 195–213.

Hunt, E. R. and B. A. Miyake. 2006. Comparison of stocking rates from remote sensing and geospatial data. *Rangeland Ecology & Management*, 59, 11–18.

Hunt, E. R. and B. N. Rock. 1989. Detection of changes in leaf water content using near- and middle-infrared refl ctances. *Remote Sensing of Environment*, 30, 43–54.

Ito, A. 2011. A historical meta-analysis of global terrestrial net primary productivity: Are estimates converging? *Global Change Biology*, 17, 3161–3175.

Jabbar, M. T. and J. Zhou. 2013. Environmental degradation assessment in arid areas: A case study from Basra Province, southern Iraq. *Environmental Earth Sciences*, 70, 2203–2214.

Jarlan, L., S. Mangiarotti, E. Mougin, P. Mazzega, P. Hiernaux, and V. L. Dantec. 2008. Assimilation of SPOT/VEGETATION NDVI data into a Sahelian vegetation dynamics model. *Remote Sensing of Environment*, 112, 1381–1394.

Jenkins, G., K. Mohr, V. Morris, and O. Arino. 1997. The role of convective processes over the Zaire- Congo basin to the southern hemispheric ozone maximum. *Journal of Geophysical Research*, 102, 18963–18980.

Jinguo, Y., N. Zheng, and C. Wang. 2006. Vegetation NPP distribution based on MODIS data and CASA model—A case study of northern Hebei Province. *Chinese Geographical Science*, 16, 334–341.

Jung, M., K. Henkel, M. Herold, and G. Churkina, (2006). Exploiting synergies of global land cover products for carbon cycle modeling. *Remote Sensing of Environment*, 101, 534–553.

Kaufman, Y. J., P. V. Hobbs, V. Kirchhoff, P. Artaxo, L. A. Remer, B. N. Holben, M. D. King, D. E. Ward, E. M. Prins, K. M. Longo, L. F. Mattos, C. A. Nobre, J. D. Spinhirne, Q. Ji, A. M. Thompson, J. F. Gleason, S. A. Christopher, and S. C. Tsay, (1998). Smoke, Clouds, and Radiation-Brazil (SCAR-B) experiment. *Journal of Geophysical Research-Atmospheres*, 103, 31783–31808.

Kaufman, Y. J., C. O. Justice, L. P. Flynn, J. D. Kendall, E. M. Prins, L. Giglio, D. E. Ward, W. P. Menzel et al. 1996a. Potential global fi e monitoring from EOSMODIS. *Journal of Geophysical Research: Atmospheres*, 103, 32215−32238.

Kaufman, Y. J., L. A. Remer, R. D. Ottmar, D. E. Ward, R. R. Li, R. Kleidman, R. S. Fraser, L. Flynn et al. 1996b. Relationship between remotely sensed fi e intensity and rate of emission of smoke: SCAR-C experiment. In *Global Biomass Burning*, ed. J. Levin, pp. 685–696. Cambridge, MA: The MIT Press.

Kauth, R. J. and G. S. Thomas. 1976. The tasseled cap—A graphic description of the spectral-temporal development of agricultural crops as seen by LANDSAT. In *LARS Symposia*, Paper 159, pp. 4B-41–4B-51. West Lafayette, IN: Purdue e-Pubs, Purdue University.

Kawamura, K., T. Akiyama, H. Yokota, and M. Tsutsumi. 2005. Monitoring of forage conditions with MODIS imagery in the Xilingol steppe, Inner Mongolia. *International Journal of Remote Sensing*, 26, 1423–1436.

Key, C. H. and N. C. Benson. 1999a. The normalized burn ratio (NBR): A Landsat TM radiometric measure of burn severity. http://nrmsc.usgs.gov/research/ndbr.htm (accessed on March 31, 2014).

Key, C. H. and N. C. Benson. 1999b. Measuring and remote sensing of burn severity. In *Proceedings of the Joint Fire Science Conference*, eds. L. F. Neuenschwander, K. C. Ryan, and G. E. Goldberg, Vol. II, p. 284. Boise, ID: University of Idaho and the International Association of Wildland Fire.

Key, C. H. and N. C. Benson. 2006. Landscape assessment: Ground measure of severity, the Composite Burn Index, and remote sensing of severity, the Normalized Burn Index. In *FIREMON: Fire Effects Monitoring and Inventory System, For. Serv. Gen. Tech. Rep. RMRS-GTR-164*, eds. D. C. Lutes et al., pp. CD: LA1–LA51. Ogden, UT: USDA For. Serv. Rocky Mt. Res. Stn.

Koch, A., A. McBratney, M. Adams, D. Field, R. Hill, J. Crawford, B. Minasny, R. Lal et al. 2013. Soil security: Solving the global soil crisis. *Global Policy*, 4, 434–444.

Lambin, E. F., B. L. Turner, and J. Helmut. 2001. The causes of land-use and land-cover change: Moving beyond the myths. *Global Environmental Change*, 11, 261–269.

Le, Q. B., L. Tamene, and P. L. G. Vlek. 2012. Multi-pronged assessment of land degradation in West Africa to assess the importance of atmospheric fertilization in masking the processes involved. *Global Planetary Change*, 92, 71–81.

Le Houérou, H. N. 1984. Rain-use efficiency: A unifying concept in arid-land ecology. *Journal of Arid Environments*, 7, 213–247.

Le Houérou, H. N., R. L. Bingham, and W. Skerbek. 1988. Relationship between the variability of primary production and the variability of annual precipitation in world arid lands. *Journal of Arid Environments*, 15, 1–18.

Lee, T. E., S. Miller, F. J. Turk, C. Schueler, R. Julian, S. Deyo, P. Dills, and S. Wang. 2006. The NPOESS VIIRS day/night visible sensor. *Bulletin of the American Meteorological Society*, 87, 191–199.

Lepers, E., E. F. Lambin, A. C. Janetos, R. DeFries, F. Achard, N. Ramankutty, and R. J. Scholes. 2005. A synthesis of information on rapid land-cover change for the period 1981–2000. *BioScience*, 55, 115–124.

Levitus, S., J. I. Antonov, T. P. Boyer, and C. Stephens. 2000. Warming of the world ocean. *Science*, 287, 2225–2229.

Li, S., C. Potter, and C. Hiatt, (2012). Monitoring of Net Primary Production in California Rangelands Using Landsat and MODIS Satellite Remote Sensing. *Natural Resources, Vol.03No.02*, 10.

Loboda, T. V., N. H. F. French, C. Hight-Harf, L. Jenkins, and M. E. Miller. 2013. Mapping fi e extent and burn severity in Alaskan tussock tundra: An analysis of the spectral response of tundra vegetation to wildland fi e. *Remote Sensing of Environment*, 134, 194–209.

Loboda, T. V., L. Giglio, L. Boschetti, and C. O. Justice. 2012. Regional fi e monitoring and characterization using global NASA MODIS fi e products in dry lands of Central Asia. *Frontiers in Earth Science*, 6, 196–205.

Lopez-Garcia, M. J. and V. Caselles. 1991. Mapping burns and natural reforestation using Thematic Mapper data. *Geocarto International*, 6, 31–37.

Loveland, T. R., B. C. Reed, J. F. Brown, D. O. Ohlen, L. Yang, and J. W. Merchant. 2000. Development of a global land cover characteristics database and IGBP DISCover from 1 km AVHRR data. *International Journal of Remote Sensing*, 29, 3–10.

Ludwig, J. 1987. Primary productivity in arid lands: Myths and realities. *Journal of Arid Environments*, 13, 1–7.

Lund, G. H. 2007. Accounting for the worlds rangelands. *Rangelands*, 29, 3–10.

Mansour, K., O. Mutango, T. Everson, and E. Adam. 2012. Discriminating indicator grass species for rangeland degradation assessment using hyperspectral data resampled to AISA Eagle resolution. *ISPRS Journal of Photogrammetry and Remote Sensing*, 70, 56–65.

Marini, A. and M. Talbi. 2009. *Desertification and Risk Analysis Using High and Medium Resolution Satellite Data*, 271 pp. Dordrecht, the Netherlands: Springer.

Matthews, E. 1983. Global vegetation and land use: New high-resolution data bases for climate studies. *Journal of Climatology and Applied Meteorology*, 22, 474–487.

Mayaux, P., H. Eva, J. Gallego, A. H. Strahler, M. Herold, S. Agrawal, S. Naumov, E. E. D. Miranda et al. 2006. Validation of the global land cover 2000 map. *IEEE Transactions on Geoscience and Remote Sensing*, 44, 1728–1738.

McCullum, I., M. Obersteiner, S. Nilsson, and A. Shvidenko. 2006. A spatial comparison of four satellite derived 1 km global land cover datasets. *International Journal of Applied Earth Observation and Geoinformation*, 8, 246–255.

McGraw, J. F. and P. T. Tueller. 1983. Landsat computer-aided analysis techniques for range vegetation mapping. *Journal of Range Management*, 36, 627–631.

Metternicht, G. 1996. *Detecting and Monitoring Land Degradation Features and Processes in the Cochabamba Valleys, Bolivia*. Enschede, the Netherlands: International Institute for Geo-Information Science and Earth Observation, ITC Publication No.36.

Metternicht, G. and J. Zinck. 2003. Remote sensing of soil salinity: Potentials and constraints. *Remote Sensing of Environment*, 85, 1–20.

Metternicht, G. and J. Zinck. 2009. *Remote Sensing of Soil Salinization—Impact on Land Management*. London, U.K.: CRC Press.

Millennium Ecosystem Assessment. 2005. *Ecosystems and Human Well-Being: Desertification Synthesis*. Washington, DC: Island Press.

Miller, J. D. and A. E. Thode. 2007. Quantifying burn severity in a heterogeneous landscape with a relative version of the delta Normalized Burn Ratio (dNBR). *Remote Sensing of Environment*, 109, 66–80.

Miura, T., A. Huete, and H. Yoshioka. (2006). An empirical investigation of cross-sensor relationships of NDVI and red/near-infrared reflectance using EO-1 Hyperion data. *Remote Sensing of Environment*, 100, 223–236.

Myneni, R.B., S. Hoffman, Y. Knyazikhin, J.L. Privette, J. Glassy, Y. Tian, Y. Wang, X. Song, Y. Zhang, G. R. Smith, A. Lotsch, M. Friedl, J. T. Morisette, P. Votava, R. R. Nemani, and S. W. Running, (2002). Global products of vegetation leaf area and fraction absorbed PAR from year one of MODIS data. *Remote Sensing of Environment*, 83, 214–231.

Myneni, R. B., R. R. Nemani, and S. Running. 1997. Estimation of global leaf area index and absorbed PAR using radiative transfer models. *IEEE Transactions on Geoscience and Remote Sensing*, 35, 1380–1393.

Nachtergaele, F., M. Petri, R. Biancalani, G. Van Lynden, and H. Van Velthuizen, (2010). Global Land Degradation Information System (GLADIS). Beta Version. An Information Database for Land Degradation Assessment at Global Level. Land Degradation Assessment in Drylands Technical Report, (17).

National Wildfire Coordinating Group (NWCG). 2012. Glossary of Wildland fire terminology. http://www.nwcg.gov/pms/pubs/glossary/ (accessed March 31, 2014).

Nkonya, E., J. von Braun, A. Mirzabaev, Q. B. Le, H. Y. Kwon, and O. Kurui. 2013. Economics of land degradation initiative: Methods and approach for global and national assessments. ZEF-discussion papers on development policy No. 183, Bonn, Germany, pp. 40.

Oldeland, J., W. Dorigo, D. Wesuls, and N. Jürgens. 2010. Mapping bush encroaching species by seasonal differences in hyperspectral imagery. *Remote Sensing*, 2, 1416–1438.

Oldeman, L. R. 1998. Soil degradation: A threat to food security? Report 98/01. International Soil Reference and Information Centre, Wageningen.

Oldeman, L., R. Hakkeling, and W. Sombroek. 1991. *World Map of the Status of Human-Induced Soil Degradation: An Explanatory Note* (2nd edn.). Wageningen, the Netherlands: International Soil Reference and Information centre.

Olson, J. S. 1983. *Carbon in Live Vegetation of Major World Ecosystems*, ORNL-5862. Environmental Sciences Division Publication No. 1997. Oak Ridge, TN: Oak Ridge National Laboratory.

OpenScientist. 2011. Finalizing a Definition of "Citizen Science" and Citizen Scientists." http://www.openscientist.org/2011/09/finalizing-definition-of-citizen.html (accessed March 31, 2014).

Paltridge, G. W. and I. Barber. 1988. Monitoring grassland dryness and fire potential in Australia with NOAA/AVHRR data. *Remote Sensing of Environment*, 25, 381–394.

Parker, A. E. and E. R. Hunt. 2004. Accuracy assessment for detection of leafy spurge with hyperspectral imagery. *Journal of Range Management*, 57, 106–112.

Paruelo, J. M., H. E. Epstein, W. K. Lauenroth, and I. C. Burke. 1997. ANPP estimates from NDVI for the central grassland region of the United States. *Ecology*, 78, 953–958.

Pech, R. P., R. D. Graetz, and A. W. Davis. 1986. Reflectance modeling and the derivation of vegetation indexes for an Australian semiarid shrubland. *International Journal of Remote Sensing*, 7, 389–403.

Pickup, G. 1996. Estimating the effects of land degradation and rainfall variation on productivity in rangelands, an approach using remote sensing and models of grazing and herbage dynamics. *Journal of Applied Ecology*, 33, 819–832.

Pickup, G. and V. H. Chewings. 1988. Forecasting patterns of soil-erosion in arid lands from Landsat MSS data. *International Journal of Remote Sensing*, 9, 69–84.

Pickup, G. and B. D. Foran. 1987. The use of spectral and spatial variability to monitor cover change on inert landscapes. *Remote Sensing of Environment*, 23, 351–363.

Pickup, G. and D. J. Nelson. 1984. Use of Landsat radiance parameters to distinguish soil-erosion, stability, and deposition in arid central Australia. *Remote Sensing of Environment*, 16, 195–209.

Plummer, S., O. Arino, M. Simon, and W. Steffen. 2006. Establishing an earth observation product service for the terrestrial carbon community: The GLOBCARBON initiative. *Mitigation and Adaptation Strategies for Global Change*, 11, 97–111.

Pohl, C. and J. L. Van Genderen, (1998). Review article Multisensor image fusion in remote sensing: Concepts, methods and applications. *International Journal of Remote Sensing*, 19, 823–854.

Ponce-Hernandez, R. and P. Koohafkan. 2004. Methodological framework for land degradation assessment in drylands (LADA) (simplified version). ftp://ftp.fao.org/agl/agll/lada/LADA-Methframwk-simple.pdf (accessed March 31, 2014).

Prince, S. D. 2002. Spatial and temporal scale for detection of desertifi ation. In *Do Humans Create Deserts*, eds. J. F. Reynolds and M. Stafford-Smith, pp. 23–40. Berlin, Germany: Dahlem University Press.

Prince, S. D. and C. J. Tucker, (1986). Satellite Remote-Sensing of Rangelands in Botswana .2. Noaa Avhrr and Herbaceous Vegetation. *International Journal of Remote Sensing*, 7, 1555–1570.

Prince, S. D., I. Becker-Reshef, and K. Rishmawi. 2009. Detection and mapping of long-term land degradation using local net production scaling: Application to Zimbabwe. *Remote Sensing of Environment*, 113, 1046–1057.

Prince, S. D., K. J. Wessels, C. J. Tucker, and S. E. Nicholson. 2007. Desertifi ation in the Sahel: A reinterpretation of a reinterpretation. *Global Change Biology*, 13, 1308–1313.

Pu, R., P. Gong, Z. Li, and J. Scarborough. 2004. A dynamic algorithm for wildfi e mapping with NOAA/AVHRR data. *International Journal of Wildland Fire*, 13, 275–285.

Reeves, M. and L. S. Bagget. 2014. A remote sensing protocol for identifying rangelands with degraded productive capacity. *Ecological Indicators*, 43, 172–182.

Reeves, M. C. and J. E. Mitchell. 2011. Extent of coterminous US rangelands: Quantifying implications of differing agency perspectives. *Rangeland Ecology and Management*, 64, 1–12.

Reeves, M. C., J. C. Winslow, and S. W. Running. 2001. Mapping weekly rangeland vegetation productivity using MODIS algorithms. *Journal of Range Management*, 54, 90–105.

Reeves, M. C., M. Zhao, and S. W. Running. 2006. Applying improved estimates of MODIS productivity to characterize grassland vegetation dynamics. *Journal of Rangeland Ecology and Management*, 59, 1–10.

Robinove, C., J. P. S. Chavez, D. Gehring, and R. Holmgren. 1981. Arid land monitoring using Landsat albedo difference images. *Remote Sensing of Environment*, 11, 133–156.

Rollins, Matthew G. "LANDFIRE: A nationally consistent vegetation, wildland fi e, and fuel assessment." *International Journal of Wildland Fire* 18.3 (2009): 235–249.

Rouse, J. W., R. H. Haas, J. A. Schell, and D. W. Deering. 1973. Monitoring vegetation systems in the Great Plains with ERTS. In *Proceedings of the Third ERTS Symposium*, Washington, DC, pp. 309–317.

Rouse Jr., J. W., R. H. Hass, J. A. Schell, D. Deering, and J. C. Harlan. 1974. *Monitoring the Vernal Advancement and Retrogradation (Greenwave Effect) I of Natural Vegetation*, 390. College Station, TX: Remote Sensing Center, Texas A&M University.

Roy, D. P., L. Boschetti, C. O. Justice, and J. Ju. 2008. The collection 5 MODIS burned area product—Global evaluation by comparison with the MODIS active fi e product. *Remote Sensing of Environment*, 112, 3960–3707.

Running, S. W., D. D. Baldocchi, D. P. Turner, S. T. Gower, P. S. Bakwin, and K. A. Hibbard. 1999. A global terrestrial monitoring network integrating tower fluxes, flask sampling, ecosystem modeling and EOS satellite data. *Remote Sensing of Environment*, 70, 108–127.

Running, S. W., R. R. Nemani, F. A. Heinsch, M. Zhao, M. Reeves, and H. Hashimoto. 2004. A continuous satellite-derived measure of global terrestrial primary production. *Bioscience*, 54, 547–560.

Safriel, U. 2009. Deserts and desertifi ation: Challenges but also opportunities. *Land Degradation and Development*, 20, 353–366.

Sant, E. D., G. E. Simonds, R. D. Ramsey, and R. T. Larsen, (2014). Assessment of sagebrush cover using remote sensing at multiple spatial and temporal scales. *Ecological Indicators*, 43, 297–305.

Scepan, J. 1999. Thematic validation of high-resolution global land-cover data sets. *Photogrammetric Engineering and Remote Sensing*, 65, 1051–1060.

Scheftic, W., X. Zeng, P. Broxton, and M. Brunke, (2014). Intercomparison of seven NDVI products over the United States and Mexico. *Remote Sensing*, 6, 1057–1084.

Schueler, C., J. E. Clement, L. Darnton, F. DeLuccia, T. Scalione, and H. Swenson. 2003. VIIRS sensor performance. International Geoscience And Remote Sensing Symposium Proceedings, Volume 1. Toulouse, France. p: 369–372.

Scott, J. M., F. Davis, B. Csuti, R. Noss, B. Butterfi ld, C. Groves, H. Anderson, S. Caicco et al. 1993. Gap analysis—A geographic approach to protection of biological diversity. *Wildlife Monographs*, 123, 1–41.

Sexton, J. O., X. P. Song, M. Feng, P. Noojipady, A. Anand, C. Huang, D. Kim, K. M. Collins et al. 2013. Global, 30-m resolution continuous fi lds of tree cover: Landsat-based rescaling of MODIS vegetation continuous fi lds with lidar-based estimates of error. *International Journal of Digital Earth*, 6(5), 427–448.

Shen, L., Z. Li, and X. Guo. 2014. Remote sensing of leaf area index (LAI) and a spatiotemporally parameterized model for mixed grasslands. *International Journal of Applied Science and Technology*, 4, 46–61.

Shoshanya, M., N. Goldshleger, and A. Chudnovsky. 2013. Monitoring of agricultural soil degradation by remote-sensing methods: A review. *International Journal of Remote Sensing*, 34, 6152–6181.

Silva, J. M. N., A. C. L. Sá, and J. M. C. Pereira. 2005. Comparison of burned area estimate derived from SPOT-VEGETATION and Landsat ETM+ data on Africa: Influence of spatial pattern and vegetation type. *Remote Sensing of Environment*, 2, 188–201.

Silverton, J. 2009. A new dawn for citizen science. *Trends in Ecological Evolution*, 24, 467–201.

Skidmore, A. K. and J. G. Ferwerda. 2008. Resource distribution and dynamics. In *Resource Ecology: Spatial and Temporal Dynamics of Foraging*, eds. H. H. T. Prins and F. van Langevelde. Wageningen, the Netherlands: Springer.

Socientize Project (2013–12–01). 2013. Green Paper on Citizen Science: Citizen Science for Europe: Towards a better society of empowered citizens and enhanced research. Socientize consortium.

Society for Range Management [SRM], Glossary Update Task Group. 1998. *Glossary of Terms Used in Range Management* (4th edn.), 32 pp. Denver, CO: Society for Range Management.

Sow, M., C. Mbow, C. Hély, R. Fensholt, and B. Sambou, (2013). Estimation of herbaceous fuel moisture content using vegetation indices and land surface temperature from MODIS data. *Remote Sensing*, 5, 2617–2638.

Steven, M. D., T. J. Malthus, F. Baret, H. Xu, and M. J. Chopping. 2003. Intercalibration of vegetation indices from different sensor systems. *Remote Sensing of Environment*, 88, 412–422.

Stuth, J. W., J. Angerer, R. Kaitho, K. Zander, A. Jama, C. Heath, J. Bucher, W. Hamilton, R. Conner, D. Inbody. (2003a) The Livestock Early Warning System (LEWS): Blending technology and the human dimension to support grazing decisions. *Arid Lands Newsletter*, University of Arizona. Available from http://cals.arizona.edu/OALS/ALN/aln53/stuth.html (accessed 4/17/2015).

Stuth, J. W., D. Schmitt, R. C. Rowan, J. P. Angerer, K. Zander, (2003b) PHYGROW Users Guide and Technical Documentation. Texas A&M University. Available from http://cnrit.tamu.edu/physite/PHYGROW_userguide.pdf (accessed April 15, 2015).

Stuth, J.W., J. Angerer, R. Kaitho, A. Jama, R. Marambii, (2005a) Livestock early warning system for Africa rangelands. In Boken V. K., Cracknell A. P. and Heathcote R. L. (eds), *Monitoring and Predicting Agricultural Drought: A global Study*. Oxford University Press, New York, pp. 283–294.

Suits, G., W. Malila, and T. Weller. 1988. Procedures for using signals from one sensor as substitutes for signals of another. *Remote Sensing of Environment*, 25, 395–408.

Svoray, T., A. Perevolotsky, and P. M. Atkinson, (2013). Ecological sustainability in rangelands: The contribution of remote sensing. *International Journal of Remote Sensing*, 34, 6216–6242.

Tansey, K., J. M. Gregoire, E. Binaghi, L. Boschetti, P. A. Brivio, D. Ershov, S. Flasse, R. Fraser et al. 2004. A global inventory of burned area at 1 km resolution for the year 2000 derived from SPOT Vegetation data. *Climatic Change*, 67, 345–377.

Tchuenté, K., A. Thibaut, J. L. Roujean, and S. M. D. Jong. 2011. Comparison and relative quality assessment of the GLC2000, GLOBCOVER, MODIS and ECOCLIMAP land cover data sets at the African continental scale. *International Journal of Applied Earth Observation and Geoinformation*, 13, 207–219.

Telesca, L. and R. Lasaponara. 2006. Quantifying intra-annual persistent behaviour in SPOT-VEGETATION NDVI data for Mediterranean ecosystems of southern Italy. *Remote Sensing of Environment*, 101, 95–103.

Thoma, D. P., D. W. Bailey, D. S. Long, G. A. Nielsen, M. P. Henry, M. C. Breneman, and C. Montagne. 2002. Short-term monitoring of rangeland forage conditions with AVHRR imagery. *Journal of Range Management*, 55, 383–389.

Todd, S. W., R. M. Hoffer, and D. G. Milchunas. 1998. Biomass estimation on grazed and ungrazed rangelands using spectral indices. *International Journal of Remote Sensing*, 19, 427–438.

Tucker, C. J. 1979. Red and photographic infrared linear combinations for monitoring vegetation. *Remote Sensing of Environment*, 8, 127–150.

Tucker, C. J. 1980. Remote sensing of leaf water content in the near infrared. *Remote Sensing of Environment*, 10, 23–32.

Tucker, C. J., J. E. Pinzon, M. E. Born, D. A. Slayback, E. W. Pak, R. Mahoney, E. F. Vermote, and N. E. Saleous. 2005. An extended AVHRR 8-km NDVI dataset compatible with MODIS and SPOT vegetation NDVI data. *International Journal of Remote Sensing*, 26, 4485–4498.

Tucker, C. J., C. Vanpraet, E. Boerwinkel, and A. Gaston. 1983. Satellite remote sensing of total dry matter production in the Senegalese Sahel. *Remote Sensing of the Environment*, 13, 461–474.

Tueller, P. T., F. R. Honey, and I. J. Tapley. 1978. Landsat and photographic remote sensing for arid land applications in Australia. In *International Symposium on Remote Sensing of Environment, Proceedings*, Ann Arbor, Michigan. pp. 2177–2191.

United Nations Convention to Combat Desertifi ation (UNCCD). 1994. Article 2 of the Text of the United Nations Convention to Combat Desertifi ation. http://www.unccd.int/Lists/SiteDocumentLibrary/conventionText/conv-eng.pdf (accessed March 31, 2014).

UNEP. 2012. Global Environment Outlook: GEO-5. Nairobi, Kenya: United Nations Environment Programme. 551 p.

Veraverbeke, S., S. Lhermitte, W. W. Verstraeten, and R. Goossens. 2011. Time-integrated MODIS burn severity assessment using the multi-temporal differenced normalized burn ratio (dNBR(MT)). *International Journal of Applied Earth Observation and Geoinformation*, 13, 52–58.

Verbesselt, J., B. Somers, S. Lhermitte, I. Jonckheere, J. van Aardt, and P. Coppin. 2007. Monitoring herbaceous fuel moisture content with SPOT VEGETATION time-series for fi e risk prediction in savanna ecosystems. *Remote Sensing of Environment*, 108, 357–368.

Vitousek, P. M. 1992. Global environmental change: An introduction. *Annual Review of Ecology, Evolution, and Systematics*, 23, 1–14.

Vlek, P., Q. B. Le, and L. Tamene. 2010. Assessment of land degradation, its possible causes and threat to food security in Sub-Saharan Africa. In *Food Security and Soil Quality*, eds. R. Lal and B. A. Stewart, pp. 57–86. Boca Raton, FL: CRC Press.

Vogl, R. 1979. Some basic principles of grassland fi e management. *Environmental Management*, 3, 51–57.

Washington-Allen, R. A., N. E. West, R. D. Ramsey, and R. A. Efroymson. 2006. A protocol for retrospective remote sensing-based ecological monitoring of rangelands. *Rangeland Ecology Management*, 59, 19–29.

Weber, G. E., K. Moloney, and F. Jeltsch. 2000. Simulated long-term vegetation response to alternative stocking strategies in savanna rangelands. *Plant Ecology*, 150, 77–96.

Wenze, Y., B. Tan, D. Huang, M. Rautiainen, N. V. Shabanov, Y. Wang, J. L. Privette, K. F. Huemmrich et al. 2006. MODIS leaf area index products: From validation to algorithm improvement. *IEEE Transactions on Geoscience and Remote Sensing*, 44, 1885–1898.

Wessels, K. J. (2009). Letter to the Editor-Comments on 'Proxy global assessment of land degradation' by Bai et al. (2008). *Soil Use and Management*, 25, 91–92.

Wessels, K. J., S. D. Prince, P. E. Frost, and D. van Zyl. 2004. Assessing the effects of human-induced land degradation in the former homeland of northern South Africa with a 1 km AVHRR NDVI time-series. *Remote Sensing of Environment*, 91, 47–67.

Wessels, K. J., S. D. Prince, J. Malherbe, J. Small, P. E. Frost, and D. van Zyl. 2007. Can human-induced land degradation be distinguished from the effects of rainfall variability? A case study in South Africa. *Journal of Arid Environments*, 68, 271–297.

Wilson, M. F. and A. Henderson-Sellers. 1985. A global archive of land cover and soils data for use in general circulation climate models. *International Journal of Climatology*, 5, 119–143.

Wooster, M. J., G. Roberts, G. Perry, and Y. J. Kaufman. 2005. Retrieval of biomass combustion rates and totals from fire radiative power observations: Calibration relationships between biomass consumption and fire radiative energy release. *Journal of Geophysical Research: Atmospheres*, 110, 1–24.

Wylie, B. K., E. A. Fosnight, T. G. Gilmanov, A. B. Frank, J. A. Morgan, M. R. Haferkamp, and T. P. Meyers. 2007. Adaptive data-driven models for estimating carbon fluxes in the northern Great Plains. *Remote Sensing of Environment*, 106, 399–413.

Xiao, J., Q. Zhuang, D. D. Baldocchi, B. E. Law, A. D. Richardson, J. Chen, R. Oren, G. Starr et al. 2008. Estimation of net ecosystem carbon exchange for the conterminous United States by combining MODIS and AmeriFlux data. *Agricultural and Forest Meteorology*, 148, 1827–1847.

Xie, Y., Z. Sha, and M. Yu, (2008). Remote sensing imagery in vegetation mapping: A review. *Journal of Plant Ecology*, 1, 9–23.

Yebra, M., E. Chuvieco, and D. Riaño, (2008). Estimation of live fuel moisture content from MODIS images for fi e risk assessment. *Agricultural and Forest Meteorology*, 148, 523–536.

Yin, H., T. Udelhoven, R. Fensholt, D. Pflugmacher, and P. Hostert, (2012). How Normalized Difference Vegetation Index (NDVI) Trends from Advanced Very High Resolution Radiometer (AVHRR) and Systeme Probatoire d'Observation de la Terre VEGETATION (SPOT VGT) Time Series Differ in Agricultural Areas: An Inner Mongolian Case Study. *Remote Sensing*, 4, 3364–3389.

Yost, E. and S. Wenderoth. 1969. Ecological applications of multispectral colour aerial photography. In *Remote Sensing in Ecology*, ed. P. L. Johnson, pp. 46–62. Athens, GA: University of Georgia Press.

Yu, L., L. Zhou, W. Liu, and H. K. Zhou. 2011. Using remote sensing and GIS technologies to estimate grass yield and livestock carrying capacity of alpine grasslands in Golog Prefecture China. *Pedosphere*, 17, 419–424.

Zhang, L., D. J. Jacob, X. Liu, J. A. Logan, K. Chance, A. Eldering, and B. R. Bojkov, (2010). Intercomparison methods for satellite measurements of atmospheric composition: Application to tropospheric ozone from TES and OMI. *Atmos. Chem. Phys.*, 10, 4725–4739.

Zhao, M., S. Running, F. Heinsch, and R. Nemani,(2011). MODIS-Derived Terrestrial Primary Production. In B. Ramachandran, C.O. Justice, & M.J. Abrams (Eds.), *Land Remote Sensing and Global Environmental Change* (pp. 635–660): Springer New York.

Zhao, M. and S. W. Running. 2010. Drought induced reduction in global terrestrial net primary production from 2000 to 2009. *Science*, 329, 940–943

Zhu, L. and J. Southworth. 2013. Disentangling the relationships between net primary production and precipitation in Southern Africa savannas using satellite observations from 1982 to 2010. *Remote Sensing*, 5, 3803–3825.

Zika, M. E. and K. H. Erb. 2009. The global loss of net primary production resulting from human-induced soil degradation in drylands. *Ecological Economics*, 69, 310–388.